Pressure and Temperature Dependence of the Reaction of Vinyl Radical with Alkenes III: Measured Rates and Predicted Product Distributions for Vinyl + Butene

C. Franklin Goldsmith,[a] Huzeifa Ismail,[b,†] William H. Green[*,a]

[a] *Department of Chemical Engineering, Massachusetts Institute of Technology, Cambridge, MA 02139, USA;*

[b] *Department of Chemistry, Massachusetts Institute of Technology, Cambridge, MA 02139, USA;*

† Present address: Baker Petrolite, Sugar Land, TX, 77478
* Authors to whom correspondence should be addressed to whgreen@mit.edu (William H. Green)

Abstract

This work reports experimental and theoretical first-order rate constants for the reaction of vinyl radical with C_4H_8 alkenes: 1-butene, 2-butene, and iso-butene. The experiments are performed over a temperature range of 300 K to 700 K at 100 Torr. Vinyl radicals (H_2C=CH) were generated by laser photolysis of vinyl iodide (C_2H_3I) at 266 nm, and time-resolved absorption spectroscopy was used to probe vinyl radicals at 423.2 and 475 nm. Weighted Arrhenius fits to the experimental rate coefficients for 1-butene (k_1), 2-butene (k_2), and iso-butene (k_3) yield $k_1 = (1.3\pm0.3)\times 10^{-12}$ cm^3 molecules^{-1} s^{-1} exp[-(2200 ± 120) K/T]; $k_2 = (1.7\pm0.3)\times 10^{-12}$ cm^3 molecules^{-1} s^{-1} exp[-(2610 ± 120) K/T]; $k_3 = (1.0\pm0.1)\times 10^{-12}$ cm^3 molecules^{-1} s^{-1} exp[-(2130 ± 50) K/T], respectively. C_6H_{11} potential energy surfaces (PES) for each system were calculated using the G3 method. RRKM/ME simulations were performed for each system to predict pressure dependent rate coefficients and branching fractions for the major channels. A generic rate rule for vinyl addition to various alkenes is recommended; a similar rate rule for the abstraction of H

atoms by vinyl from alkenes is also provided. Some of the vinyl addition reactions exhibit anomalous Evans-Polanyi plots, similar to those reported for previous methyl addition reactions.

Introduction

Reactions involving vinylic radicals are important in combustion processes.[1] The simplest radical of this class is vinyl (C_2H_3), which has a pivotal role in the competition between oxidation and molecular weight growth chemistry leading to soot formation. At high temperatures, vinyl rapidly decomposes to acetylene.[2] In O_2 starved environments at lower temperatures, vinyl either will add to unsaturated hydrocarbons, or it will abstract an H-atom; these two competing reactions will create a mixture of dienes, cyclic species, and resonantly stabilized free radicals, each of which can lead to the formation of polycyclic aromatic hydrocarbons (PAH) and other early precursors of soot.[3] In contrast, if O_2 is present, vinyl reacts rapidly to form vinylperoxy, which after several fast chemically-activated isomerization reactions decomposes to HCO + CH_2O, and thence to CO or CO_2.[4] Thus, the relative rates of these addition, abstraction, and oxidation reactions of vinyl are central in the determination of when various fuels will form soot and when they form complete combustion products. Despite its importance, relatively little experimental work has been performed on vinyl chemistry. The only vinyl + alkene reactions that have been studied experimentally are vinyl + ethene[5-7] and vinyl + propene[8]. These recent studies[7,8] indicated a difference of roughly 2 kcal/mol in the activation energy, E_a, and factor of two difference in the A-factor between the vinyl + propene and vinyl + ethene chemical systems. No experimental or theoretical data have been reported on the rate for vinyl + butenes:

$C_2H_3 + 1\text{-}C_4H_8 \xrightarrow{k_1}$ products (1)

$C_2H_3 + 2\text{-}C_4H_8 \xrightarrow{k_2}$ products (2)

$C_2H_3 + \text{iso-}C_4H_8 \xrightarrow{k_3}$ products (3)

In the present work, vinyl iodide is used as a clean source to generate vinyl radicals. The rate coefficient for the reaction of C_2H_3 with 1-butene, 2-butene, and iso-butene has been measured over a temperature range of 300 K to 700 K at the pressure of 100 Torr. Detailed quantum calculations are also reported and compared with experimental results. The calculations reveal pressure-dependent product ratios, which were not measured experimentally. The goals of the present work are to establish generic rules for both the addition and H-abstraction reaction rate constants of vinyl with various alkenes.

Experimental Procedures

The experimental apparatus has been described previously[7], therefore only a brief summary will be given. Vinyl radicals (C_2H_3) were generated via laser photolysis of vinyl iodide at 266 nm:

$$C_2H_3I + h\nu\ (266\ \text{nm}) \rightarrow I + C_2H_3 \quad (4)$$

Photolysis pulses were generated by frequency-doubling the 532 nm output of a short pulse (2 ns) Nd:YAG laser. Vinyl radicals were detected by multiple pass laser absorption at one of two absorption lines, 423.2 nm or 475.0 nm. [9-11] The detection

wavelength was generated using a mode-locked Ti:Sapphire laser (1.2 ps at 80 MHz) pumped by a 532 nm diode-pumped solid state continuous-wave (CW) laser. The output of the Ti:Sapphire laser was frequency-doubled using a BBO crystal. The laser pulses every 12 ns, providing an effective continuous probe of the vinyl radical decay, which occurs on a much longer time scale[7,8].

The spectral range of the laser, when used with a harmonic generator, covers most of the visible wavelengths allowing for the detection of a wide array of organic radical species. The line width of the laser is 13 cm^{-1} in the 400 nm detection region. The excellent stability of this laser system allows accurate measurement of rate constants from the microsecond-to-millisecond time scale. A Herriott-type multi-pass resonator is used to increase path length up 40 meters. An Ocean Optics spectrometer (0.1 nm FWHM) was used to determine the output wavelength. The spectrum of vinyl radical is ideal for such a probe laser, because its absorption features are broader than the laser FWHM, yet still narrow enough to allow tuning off resonance. The off-resonance background signal contains contributions arising from thermal lensing; the vinyl concentration is taken to be proportional to the difference in absorption between traces taken on- and off-resonance.

The experiments were carried out in a 160 cm long temperature-controlled stainless steel flow reactor. To improve the signal-to-noise ratio, a balanced detection scheme was used where a reference beam (I_0) that does not pass through the reactor is subtracted from the probe beam (I) via a low-noise differential amplifier.

To maintain a constant flow of the reactant and buffer gases, calibrated mass flow controllers were used. The internal pressure of the reactor is measured by a capacitance

manometer and controlled via an automated butterfly valve. The flow reactor was housed in a cylindrical oven. Additional resistive heating was supplied to the reactor entrance and exit region. The entrance, center, and exit temperatures were monitored using K-type thermocouples which were fed into three independent PID controllers to maintain a uniform, constant temperature (± 5 K).

Vinyl Iodide was purchased from Oakwood Products Inc ($C_2H_3I \geq 90.0\%$) and was purified by repeated freeze-pump-thaw cycles. Additional gas-phase chemicals were purchased from following suppliers and were used without further purifications: 1-butene ≥ 99.0% (2.0 grade from Advanced Gas Technologies Inc.), 2-butene ≥ 99.0% (2.0 grade from Advanced Gas Technologies Inc.) Iso-butene ≥ 99.0% (2.0 grade from Advanced Gas Technologies Inc.), He ≥ 99.999% (5.0 grade, Airgas). The 2-butene is a mix of the cis and trans isomers, 50% ±15% trans.

All the experiments were performed between 300 K to 700 K and at a pressure of 100 Torr. To maintain pseudo-first-order conditions, alkene concentrations were in large excess over vinyl concentration. This ensured that the pseudo-first order decays were at least five times faster than the decay without added alkenes. For most of the experiments, vinyl iodide concentrations were maintained at $[C_2H_3I] = 1 \times 10^{15}$ molecules cm^{-3}. Some experiments were performed at several concentrations of vinyl by varying photolysis laser intensity and C_2H_3I concentration. It was found that the rate constants did not depend on $[C_2H_3I]$ or on photolysis energy, confirming the validity of a pseudo-first-order approximation and suggesting a negligible role for photolytic interferences. Typically, the photolysis laser pulsed once per second. Only ~ 0.2 % of vinyl iodide dissociates on each pulse. In most experiments, flow rates were sufficient to completely

refresh the cell every 3-5 seconds. To confirm that the products from previous shots were not interfering with the reaction, the flow rate was increased for several experiments so that the cell was refreshed every second. The results were indistinguishable from experiments in which the cell was refreshed every 3-5 seconds.

To determine $k_{1\text{-}3}$, the decay rate of C_2H_3 was measured at several alkene concentrations. The raw data, as shown in Figure 1a, were fit to a single exponential decay, yielding a pseudo-first order rate constant, k'. Rate constants were taken from the slope of a plot of k' versus $[C_4H_8]$, which yielded a linear slope, as shown in Figure 1b. The effective rate constant k_0, represented by the zero-alkene intercept of this plot, is attributable to all other loss processes for vinyl radical, including self-reaction, reaction with I atoms, reaction with vinyl iodide, and diffusion out of the probe beam. The measured values for k_0 reported in Tables 1-3 are comparable with what would be expected from the vinyl self reaction[12]. The uncertainty limits of k' shown in Figure 1 represent the statistical uncertainty resulting from the fit of the C_2H_3 decay data to a single exponential. Alkene concentrations used were large enough that the error in simply including the second-order contribution from self-reaction in the intercept was small. Extracting k' from the first-order component of a fit to the functional form for a combined first- and second-order decay resulted in identical values of k_1 to within experimental uncertainty.

Theory

The optimized geometries and zero-point corrected energies for the stationary points, transition states, and product channels on the C_6H_{11} potential energy surface

(PES) were calculated using the G3 compound method[13]. The HF/6-31G(d) vibrational frequencies from the G3 calculations were replaced with subsequent B3PW91/6-311++G(3df,pd) calculations to improve the accuracy of the vibrational partition function and density of state calculations. Conformers for each isomer were treated as hindered internal rotors. The potential barrier for each hindered rotor, here assumed to be any single carbon-carbon bond not included in a ring, was calculated at the B3PW91/6-31+G(d,p) level. A relaxed scan along the dihedral angle in 10 degree increments was performed, and the resulting potential barrier was fit to a Fourier series. The partition function and density of state for each rotor was treated as a one-dimensional hindered rotor with a semi-classical Pitzer-Gwinn[14] –like approximation:

$$Q = \frac{Q_{\text{classical hindered rotor}} Q_{\text{quantum harmonic oscillator}}}{Q_{\text{classical harmonic oscillator}}} \qquad (5)$$

The effective moment of inertia used for each rotor was $I^{(2,3)}$ evaluated at the equilibrium geometry. Tunneling was included for all transition states by use of an Eckart approximation[15]. For energy transfer in the master equation, a single-exponential down model was used, with an average ΔE_{down} for He given by 100 cm^{-1} $(T/298)^{0.8}$ [16,17]. The collision frequency was estimated using a Lennard-Jones model, with LJ parameters of σ = 6.25 Å and ε = 238.4 cm^{-1} for all C_6H_{11} isomers. The LJ parameters for the C_6H_{11} isomers were estimated from literature values for n-C_6H_{12}[18]. If these values were replaced by values for 1- C_4H_8, σ = 5.28 Å and ε = 209.9 cm^{-1}, the change in rate coefficients was typically less than 40%. The same source was used for the He bath gas LJ-parameters: σ = 2.55 Å and ε = 6.95 cm^{-1}. For the C_6H_{11}-He complex, σ was calculated by the arithmetic mean of the values for the two species, and ε was calculated by the geometric mean.[18] The same calculations were repeated at higher pressures (0.1 to

100 atm in N_2, with ΔE_{down} for N_2 given by 400 cm^{-1} $(T/298)^{0.8}$, σ = 3.74 Å, and ε = 56.99 cm^{-1}); the results of these calculations are available online in the Supporting Information. All G3 and DFT calculations were performed using the Gaussian 03 software package.[19] Additional coupled cluster calculations were done using MOLPRO[20]. Doublet species wave functions were unrestricted for both the energy and frequency calculations. An RRKM/ME program package, VariFlex[21], was used to calculate the density of states, microcanonical rate constants, and the pressure- and temperature-dependent rate constants for Reactions 1, 2 and 3, based on the potential energy surfaces shown in Figure 2, Figure 4, and Figure 7.

Results

Vinyl + 1-butene

The measured values for k_1 over the temperature range of 300 – 700 K are given in Table 1. An Arrhenius fit to the measured rate coefficient for Reaction 1 at 100 Torr, weighted by the uncertainties in the individual data points, yields

$$k_1 = (1.3\pm0.3)\times 10^{-12}\ cm^3\ molecules^{-1}\ s^{-1} \exp[-(2200 \pm 120)\ K/T] \quad (6)$$

The error limits in the Arrhenius equation are the 95% confidence intervals. A better fit to the observed data is given by a modified Arrhenius rate equation with the temperature exponent fixed at 1.7:

$$k_1 = (9\pm2)\times 10^{-13}\ cm^3\ molecules^{-1}\ s^{-1}\ (T/1000)^{1.7} \exp[-(1430 \pm 110)\ K/T] \quad (5)$$

The justification for the choice of temperature exponent is described below in the first section on rate rules. The measured values, the modified-Arrhenius fit, and the

computed high-pressure limits for the major and minor addition channels and the abstraction channel are shown in Figure 3a.

The potential surface calculated for vinyl + 1-butene is shown in Figure 2 and in Table 4 & 5. A detailed PES for vinyl + 1-butene is provided because this reaction is the most likely to form an endo-cyclic six-member ring, cyclohexyl radical, as well as the exo-cyclic five-member ring, cyclopentylmethyl radical, both of which could be particularly important in PAH chemistry. Although it is possible for four- and other five-member rings to be formed, they were not included in the master equation calculation, because they are not expected to be formed at significant rates[8].

The vinyl radical and 1-butene can react via three distinct low-barrier transition states:

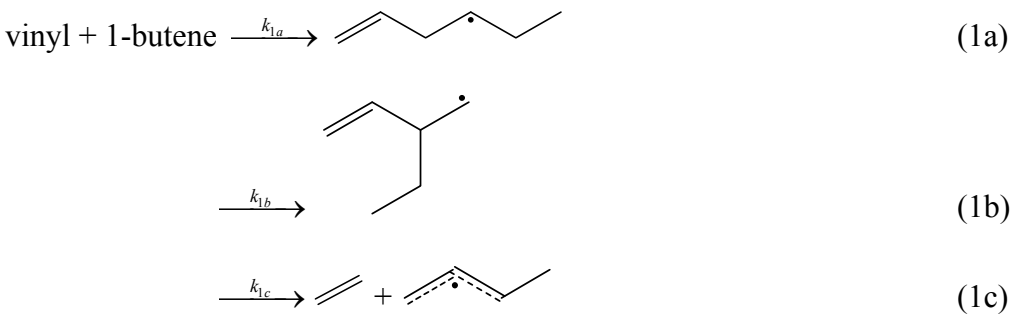

(1a)

(1b)

(1c)

The lowest energy path for Reaction 1 is reaction 1a, in which the vinyl radical forms a single bond with carbon 1 (i.e. the "head") in 1-butene, via TS 1 (see Table 5 for a complete list of transition states for vinyl + 1-butene). The second possible reaction, 1b, is when the vinyl radical forms a single bond with carbon 2 (i.e. the "tail") in 1-butene via TS 2. Reaction 1c is when the vinyl radical abstracts an H directly from the Carbon 3 in 1-butene, yielding ethene and 1-methyl-allyl radical, via TS 3. Other direct H-abstractions are possible but were not considered because the barriers were comparatively too high: e.g. the barrier for H-abstraction from the methyl group in 1-

butene is 5 kcal/mol higher than the barrier for TS 3. In addition to the three reactions listed above, rate coefficients are calculated for six chemically activated channels:

$$\text{vinyl + 1-butene} \xrightarrow{k_{1d}} \text{1,4-pentadiene + methyl} \quad (1d)$$

$$\xrightarrow{k_{1e}} \text{1,3-hexadiene + H} \quad (1e)$$

$$\xrightarrow{k_{1f}} \text{1,3-butadiene + ethyl} \quad (1f)$$

$$\xrightarrow{k_{1g}} \text{allyl + propene} \quad (1g)$$

$$\xrightarrow{k_{1h}} \text{Cyclohexene + H} \quad (1h)$$

$$\xrightarrow{k_{1i}} \text{methylene-cyclopentane + H} \quad (1i)$$

Channels 1d and 1e are formed from β-scission from 5-hexen-3-yl, and 1f is the result of β-scission from the other entrance adduct, 2-ethyl-3-buten-1-yl; Channel 1g is the result of rapid isomerization between 5-hexen-3-yl ↔ 1-hexen-1-yl ↔ 5-hexen-2-yl followed by β-scission; and Channels 1h and 1i are the result of rapid isomerization between 5-hexen-3-yl ↔ 1-hexen-1-yl ↔ 5-hexen-1-yl ↔ cyclohexyl/cyclopentylmethyl followed by β-scission.

A list of the species and their energies relative to the reactants are listed in Table 4; a corresponding list of the transition states and their energies are listed in Table 5. Because of the high barriers to isomerization, neither 1-propyl-allyl nor 1-methyl-1-ethyl-allyl was included in the master equation calculation. Similarly, the product channel 2-ethyl-1,3-butadiene + H was not included, since the barrier is higher than the reactant energy and is several kcal/mol higher than competing dissociation channels.

The RRKM/ME results are shown in Figure 3b. For temperatures below 400 K, the eigenvalue decomposition resulted in at least one positive eigenvalue. This result, not uncommon for low temperature systems [17,22], is unphysical, so RRKM/ME results at these temperatures are not reported. By 400 K, only negative eigenvalues were calculated. The isomer 2-hexen-2-yl has isomerization barriers below reactants in energy; however, including this species in the PES made no difference to the final rate coefficients. Consequently, this isomer was omitted from the master equation calculations to improve numerical accuracy. Based upon an analysis of the eigenvalues, the two initial adducts, 5-hexen-3-yl and 2-ethyl-3-buten-1-yl, are rapidly equilibrated via 2-ethyl-cyclopropylmethyl above 350 K.

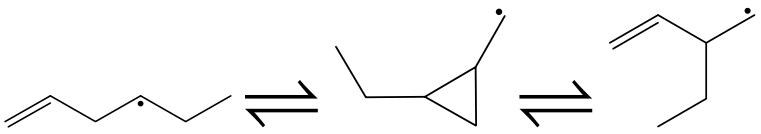

At low temperatures, the major products will be the collisionally stabilized initial adducts: 5-hexen-3-yl, 2-ethyl-3-buten-1-yl, and 2-ethyl-cyclopropylmethyl. The rate of formation for 5-hexen-2-yl, although of similar stability, is three orders of magnitude slower than 5-hexen-3-yl. The proportionally low yield of this isomer can be explained by the low barrier for β-scission from 5-hexen-2yl to form allyl + propene, TS 15. This barrier is almost 2 kcal/mol below the barrier for isomerization from 1-hexen-1yl, so 5-hexen-2-yl is initially populated at energy levels in excess of the dissociation barrier. At 100 Torr of He, the collision rate is insufficient to quench 5-hexen-2-yl, and thus the rate of formation for allyl + propene is greater than the rate of stabilization of 5-hexen-2-yl at all temperatures. Neither of the other two straight-chain isomers is formed at a

significant rate. It is both energetically and entropically favorable for 1-hexen-1-yl to isomerize to 5-hexen-2-yl rather than 5-hexen-1-yl; the 5-hexen-2-yl intermediate will then undergo beta-scission to form propene + allyl, whereas the less favored 5-hexen-1-yl can either undergo 6-endo or 5-exo cyclization. The barrier to form cyclopentylmethyl from 5-hexen-1-yl is roughly 1 kcal/mol lower than the corresponding barrier to form cyclohexyl, and the RRKM calculations confirm that cyclopentylmethyl is formed at a slightly faster rate. In contrast, the subsequent barrier for H-atom beta-scission to form a cycloalkene is roughly 4 kcal/mol higher for cyclopentylmethyl than for cyclohexyl, and the RRKM calculations confirm that cyclohexene + H is formed more rapidly than methylene-cyclopentane + H. However, none of the cyclic isomers or the respective bi-molecular products is formed at a significant rate; the rate coefficients for the cyclic species were between four and five orders of magnitude slower than the fastest rate coefficient.

At 100 Torr of He, chemically-activated product formation exceeds collisional stabilization of the adducts above 600 K. At temperatures greater than 700 K, the adduct stabilization rates drop off precipitously, and the dominant product channels are 1,4-pentadiene + methyl, 1,3-butadiene + ethyl, and ethene + 1-methyl-allyl. The other allyllic channel, propene + allyl, is roughly two orders of magnitude slower.

Vinyl + 2-butene

The measured values for k_2 between 300 – 700 K are given in Table 2. An Arrhenius fit to the measured rate coefficient for Reaction 2 at 100 Torr, weighted by the uncertainties in the individual data points, yields:

$$k_2 = (1.7\pm0.3)\times 10^{-12}\ \mathrm{cm^3\ molecules^{-1}\ s^{-1}} \exp[-(2610 \pm 120)\ \mathrm{K/T}] \qquad (7)$$

A better fit to the observed data is given by a modified Arrhenius rate equation with the temperature exponent fixed at 1.7:

$$k_2 = (9\pm2)\times 10^{-13}\ \text{cm}^3\ \text{molecules}^{-1}\ \text{s}^{-1}\ (\text{T}/1000)^{1.7}\ \ \exp[-\ (1750 \pm 120)\ \text{K}/\ \text{T}] \qquad (8)$$

The justification for the choice of temperature exponent is described below in the first section on rate rules. The measured values, the modified-Arrhenius fit, and the computed high-pressure limits for the addition and abstraction channels are shown in Figure 5a. The predicted pressure-dependent product channels from the VariFlex calculations are shown in Figure 5b. A detailed understanding of the potential energy surfaces for vinyl + 2-butene can be obtained by analogy from the vinyl + propene PES.[8] Those results suggest that the initial adduct must undergo several high-barrier isomerization reactions before it can form either six-member rings or five-member rings. Additionally, the 1,2 H-transfer isomerization to form 1-methyl-1-ethyl-allyl, TS 31, has a barrier height that is above the reactant energies and is more than 6 kcal/mol higher than the competing beta-scission reaction. Consequently, although vinyl + 2-butene can form several cyclic and six-member allylic species, none of them is formed at an appreciable rate, and thus only a simple PES is provided here, shown in Figure 4. Because of the symmetry of 2-butene, there is only one primary adduct; hence there is no need to calculate the isomerization via 2,3-dimethyl-cyclopropylmethyl (which would scramble isotopic labels). The vinyl radical and 2-butene can react via two distinct low-barrier transition states:

vinyl + 2-butene $\xrightarrow{k_{2a}}$ 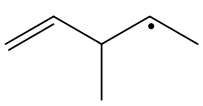 (2a)

$\xrightarrow{k_{2b}}$  (2b)

The lowest energy path for Reaction 2 is reaction 2a, in which the vinyl radical forms a single bond with carbon 2 via TS 27 and TS 28. The next lowest energy elementary reaction is 2b, in which the vinyl radical abstracts an H directly from either of the CH_3 groups in 2-butene via TS 29 and TS 30. In addition to the two reactions listed above, rate constants are calculated for two chemically activated channels:

$$\text{vinyl + 2-butene} \xrightarrow{k_{2c}} \text{1,3-pentadiene + methyl} \qquad (2c)$$

$$\xrightarrow{k_{2d}} \text{3-methyl-1,3-pentadiene + H} \qquad (2d)$$

Both of these channels result from β-scission of the initial adduct. A list of the species and their energies relative to the reactants are listed in Table 6; a corresponding list of the transition states and their energies are listed in Table 7. At 100 Torr of He, chemically-activated product formation becomes significant by 600 K. From 600 K – 1500 K, the dominant product channel is 1,3-pentadiene + methyl, followed closely by ethene + 1-methyl-allyl. The other product channel, 3-methyl-1,3-pentadiene + H, is roughly two orders of magnitude slower. Although the PES in Figure 4 shows two distinct channels for direct H-abstraction, starting from cis- or trans-2-butene, for simplicity the channels for cis-1-methyl-allyl and trans-1-methyl-allyl are lumped together as a single channel in Figure 5b. These isomers are expected to rapidly equilibrate in a flame environment.

Vinyl + iso-butene

All the experiments for the vinyl + alkenes were conducted by probing vinyl radical at 423.2 nm, except for vinyl + iso-butene. Unlike the other cases, the vinyl + iso-butene data exhibited a base-line offset, presumably due to interference by a longer-lived species. The spectrum of the baseline offset was measured from 422 nm to 480 nm. As seen in the spectrum in Figure 6 no baseline absorption is seen between 470 and 480 nm.

Vinyl radical has a weak absorption feature at 475 nm[10,11] . To avoid the spectral interference, all the measurements for k_3 were taken using this wavelength.

The conditions for the measured values for k_3 between 300 – 700 K are given in Table 3. An Arrhenius fit to the measured rate coefficient for Reaction 3 at 100 Torr, weighted by the uncertainties in the individual data points, yields

$$k_3 = (1.0\pm0.1)\times 10^{-12}\ \text{cm}^3\ \text{molecules}^{-1}\ \text{s}^{-1} \exp[-(2130 \pm 50)\ \text{K/T}] \quad (8)$$

A better fit to the observed data is given by a modified Arrhenius rate equation with the temperature exponent fixed at 1.7:

$$k_3 = (8\pm1)\times 10^{-13}\ \text{cm}^3\ \text{molecules}^{-1}\ \text{s}^{-1}\ (\text{T}/1000)^{1.7} \quad \exp[-\ (1430 \pm 50)\ \text{K/ T}] \quad (9)$$

The justification for the choice of temperature exponent is described below in the first section on rate rules. The measured values, the modified-Arrhenius fit, and the high-pressure limits for the major and minor addition channels and the abstraction channel are shown in Figure 8a. The predicted pressure-dependent product channels from the VariFlex calculations are shown in Figure 8b. A detailed understanding of the potential energy surfaces for vinyl + iso-butene can be obtained by analogy from the vinyl + propene PES.[8] Those results suggest that the initial adduct must undergo several high-barrier isomerization reactions before it can form either six-member rings or five-member rings. Additionally, the 1,2 H-transfer isomerization to form isopropyl-allyl, TS 40, has a barrier height that is above both the reactant energies and the competing beta-scission reaction. Consequently, although vinyl + iso-butene can form several cyclic and six-member allylic species, none of them is formed at an appreciable rate, and thus only a

simple PES is provided here, shown in Figure 7. The vinyl radical and iso-butene can react via three distinct low-barrier transition states:

vinyl + iso-butene $\xrightarrow{k_{3a}}$ 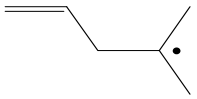 (3a)

$\xrightarrow{k_{3b}}$ 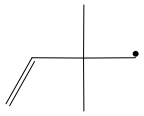 (3b)

$\xrightarrow{k_{3c}}$ 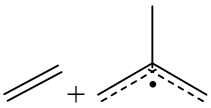 (3c)

The lowest energy path for Reaction 3 is reaction 3a, in which the vinyl radical forms a single bond with carbon 1 (i.e. the "head") in iso-butene via TS 33. The second lowest energy path is when the vinyl radical forms a single bond with carbon 2 (i.e. the "tail") in iso-butene via TS 34. Reaction 3c is when the vinyl radical abstracts an H directly from either of the methyl groups in iso-butene via TS 35. Although the barrier to this reaction is 0.5 kcal/mol higher than reaction 3b, it is roughly an order of magnitude faster, as seen in Figure 8a. In addition to the three reactions listed above, rate constants are calculated for two chemically activated channels:

vinyl + iso-butene $\xrightarrow{k_{1d}}$ 4-methyl-1,3-pentadiene + H (3d)

$\xrightarrow{k_{1e}}$ 2-methyl-1,3-butadiene + methyl (3e)

Channel 3d is the result of β-scission of the initial adduct, 2-methyl-4-penten-2-yl; channel 3e results from rapid isomerization between the initial adducts 2-methyl-4-penten-2-yl ↔ 2,2-dimethyl-cyclopropylmethyl ↔ 2,2-dimethyl-3-buten-1-yl, followed by β-scission. A list of the species and their energies relative to the reactants are listed in Table 8; a corresponding list of the transition states and their energies are listed in Table

9. Of the five vinyl + alkenes reactions studied so far, Reaction 3 is the only reaction in which the initial adduct is a tertiary radical. The increased stability of the initial adduct, and the lack of any low-energy C-C bond β-scission routes, implies that it is more difficult for chemically activated product formation to occur; at 100 Torr in He, chemical activation doesn't dominate over collisional stabilization until temperatures in excess of 850 K. Additionally, unlike vinyl + propene, 1-butene, and 2-butene, for temperatures above 700 K the dominant product channel for vinyl + iso-butene is predicted to be the direct H-abstraction, yielding ethene + 2-methyl-allyl. Between 300 and 700 K, the H-abstraction channel is computed to increase from 5% to 25% of the total rate of disappearance of vinyl.

Origin of the background absorption

We attribute the background absorption seen in Figure 6 to 2-methyl-allyl. Although the rate of H-abstraction from 1-butene is slightly faster than the abstraction from iso-butene, no baseline offset was observed at 423.2 nm for the vinyl + 1-butene experiments. One difference between these two systems is that iso-butene yields 2-methyl-allyl, whereas 1-butene leads to 1-methyl-allyl. Thus, if 2-methyl-allyl has a strong absorption at 423.2 nm and 1-methyl-allyl does not, then 2-methyl-allyl could be the source for the background absorption signal at 423.2 nm. The spectra of the methyl-allyl species have never been measured in this wavelength range. Unsubstituted allyl has a strong absorption for $\lambda \leq 408$ nm.

Discussion:

To facilitate comparison, the Arrhenius parameters for all five vinyl + alkene systems are summarized in Table 14. Between 300 and 700 K at 100 Torr of He, the

fastest rate is vinyl + propene, followed by iso-butene, 1-butene, ethene, and 2-butene. Although the experimental rates are quite similar, with less than a factor of five separating the slowest from the fastest, the ordering of the rates cannot be explained solely by molecular weight or reaction enthalpy. Three competing effects determine the relative ranking of the rates: reaction path degeneracy, rotational effects, and variations in the barrier height due to sterics and charge donation.

Reaction path degeneracy: Statistical factors, such as the external symmetry of the molecule and the number of energetically equivalent transition states, will impact the relative ranking. The external symmetry numbers for the reactants are: vinyl, 1; ethene, 4; propene and 1-butene, 1; 2-butene and iso-butene, 2. The external symmetry number for all the transition states is 1; however, the reactions for propene, 1-butene, and 2-butene each have two energetically equivalent chiral transition states. Thus, the reaction path degeneracies for the reactions are: ethene and 2-butene, 4; propene, 1-butene, and iso-butene, 2. Consequently, other things being equal, one would expect the reaction of vinyl with ethene or 2-butene to be twice as fast as the other alkenes. The importance of reaction path degeneracy is shown in Table 13.

Rotational effects: The moments of inertia for ethene and propene are significantly smaller than those of the butenes, as shown in Table 13. Consequently, due to rotational partition functions only, one would expect the reaction of vinyl + ethene to be the fastest, followed by propene, with the butenes roughly equivalent.

Barrier height: The initial adduct for vinyl + ethene is a primary radical; for propene, 1-butene, and 2-butene, the initial adduct of the major channel is a secondary radical; for iso-butene, it is a tertiary radical. Since the reaction barrier should be lower

for more stable adducts, from this argument one would expect vinyl + iso-butene to be the fastest and vinyl + ethene to be the slowest. Since the addition of vinyl to an unsubstituted CH_2 end group is less hindered than addition to a substituted carbon, one would expect propene and 1-butene to be faster than 2-butene. Additionally, one would expect 1-butene to react slightly faster than propene due to increased hyperconjugation.

In order to quantify the importance of these competing effects, quantum calculations were performed to calculate the reaction enthalpies and transition-state theory rate coefficients for all addition and abstraction rates. The reaction enthalpies and barrier heights are provided in Table 11. For each addition reaction, the geometry of the transition state indicates an early transition state, which is consistent with the low-barrier and high-exothermicity of these reactions. The geometry of the alkene is virtually unchanged: the π-bond is well preserved, with the C=C bond length in the transition state increasing by less than 0.02 Angstroms. The frontier molecular orbitals for the reactants are presented in Table 10. These calculations were performed at the RHF/aug-cc-pvtz level using MOLPRO. The vinyl radical has a low-energy singly occupied molecular orbital (SOMO). This orbital is much closer in energy to the highest occupied molecular orbital (HOMO) of the alkene than to the lowest unoccupied molecular orbital (LUMO). Consequently, the SOMO-HOMO interaction is favored, and the vinyl radical acts as a strong electrophile.

In order to put these reactions in a broader framework, it is useful to compare these results with other results for the addition of a carbon-centered radical to unsaturated hydrocarbons. In 2001 Fischer and Radom published an experimental and computational review of addition reactions involving carbon-centered radicals and alkenes[23]. This work

compared the rate constants for the addition of methyl and ten other radicals to monosubstituted and 1,1,-disubstituted alkenes. Radom and coworkers have updated the calculations for methyl addition to alkenes and compared the results with calculations for methyl addition to carbonyl and thiocarbonyl species[24]. Most recently, Sabbe et al. have published a computational study of carbon-centered radical addition to alkenes and the reverse beta-scission reactions[25]. Sabbe et al. focused primarily on methyl addition to various alkenes, but also included the addition of seventeen other radicals to ethene for comparative purposes. (Note that Tables 1-3 in Sabbe[25] incorrectly label the units for the Arrhenius A-factor as m3/mol-s; the correct units are m3/kmol-s[26]). Sabbe[25] predicts the rate constant for vinyl + ethene to be $k_{v+e} = 4.8\times 10^{-13}$ cm^3 molecules^{-1} s^{-1} exp[- 1620 K/ T]. The experimentally measured rate constant by Ismail et al[7] is $k_{v+e} = (1.2\pm0.2)\times 10^{-12}$ cm^3 molecules^{-1} s^{-1} exp[- (2310 ± 70) K/ T]. The rate constant in Sabbe[25] is roughly a factor of three higher than the experimental data at room temperature but agrees well with the 700 K data. The difference in activation energies is presumably due in part to the fact that Sabbe's rate coefficient was determined by fitting transition state theory rate constants between 198 and 398 K[26]; since the pre-exponential A-factor has a pronounced temperature dependence, the activation energy for a two-parameter Arrhenius expression will depend strongly on the temperature region over which it was fit. To facilitate comparison between methyl and vinyl addition to the first five alkenes, the barrier heights and reaction enthalpies for methyl addition to the alkenes from Henry[24] and Sabbe[25] are reproduced in Table 12. In the following discussion, the α-carbon refers to the bonding carbon, and the β-carbon is the adjacent carbon that shares the double bond in the reactant alkene. Comparing the results in Table 11 and Table 12, it is clear that for

radical addition to an unsubstituted α-carbon, the barrier height decreases with each substitution to the β-carbon. This result is expected, since each substitution to the β-carbon provides more charge donation to the double bond, which facilitates the electrophilic addition reaction. Additionally, each substitution on the β-carbon increases the stability of the product radical (from a primary to a secondary to a tertiary radical), since the radical site is localized on that β-carbon.

Further analysis of the reaction enthalpies in Table 11 and Table 12 shows an unexpected trend: as the reaction becomes more exothermic, the barrier increases. Figure 9a plots the calculated activation energy versus the reaction enthalpy for vinyl addition to an unsubstituted α-carbon. In contrast to the data, one would expect a positive slope for this Evans-Polanyi plot, typically on the order of 0.25 to 0.5. The experimental activation energies also exhibit a negative Evans-Polanyi slope, suggesting that this behavior is not limited to computational results.

The decrease in exothermicity with substitution at the β-carbon is explained as follows: Each substitution to the β-carbon in the reactant alkene stabilizes the transition state the most, the reactant the second most, and the product the least. The difference in stabilization can be explained by considering the molecular orbitals. The CH_3 (or CH_2) orbitals of the substituent mix with the π orbitals of the double bond in the alkene, thereby stabilizing the reactant. However, in the addition reaction, the π–bond in the reactant is converted to a σ-bond in the product, so the stabilizing effect due to mixing with the orbitals on substituent group is greatly reduced. The stabilizing effect due to mixing with the π bonding orbital is greater than the stabilizing effect caused by the increased charge donation when going from a primary to a secondary to a tertiary alkyl

radical. Thus, although the adduct radical is indeed stabilized by the transformation from a primary to secondary to tertiary radical, the overall reaction exothermicity decreases, because the reactant is stabilized even more. This effect can be seen more clearly by contrasting the reaction enthalpies for vinyl addition to an unsubstituted carbon with addition to a substituted carbon in Table 11. The most exothermic reaction is vinyl + ethene; the least exothermic reaction is vinyl addition to the substituted end of iso-butene. Substitution at the α-carbon stabilizes the alkene, but it does not significantly change the product radical stability. The results suggest that the stabilization associated with π–orbital mixing with each substituent on either carbon is roughly 1.3 kcal/mol, whereas the product radical is stabilized by nearest-neighbor substituents by roughly 1.0 kcal/mol. Indeed, this trend is largely predicted by basic Benson group additive thermochemistry: group additivity predicts that the exothermicity should decrease with substitution, and that addition to an unsubstituted carbon is more exothermic than addition to a substituted carbon.

In contrast to addition to unsubstituted carbons, addition to substituted carbons does not exhibit a negative Evans-Polanyi slope, as shown in Figure 9b. Here the dominant effect is steric hindrance in the transition state. As mentioned at the beginning of the discussion, the addition of vinyl radicals to alkenes are characterized by an early transition state. For addition to an unsubstituted carbon, the angle of attack for the radical center relative to the double bond is close to the value in the product: 108.5° in the transition state vs. 113.2° in the product. For addition to a substituted carbon, in contrast, the angle of attack is decreased by five degrees: 103.3° for propene and 1-butene and 98.6° for iso-butene. The addition of each carbon atom to the bonding site

creates a steric hindrance that constrains the angle of attack, thereby increasing the barrier by roughly 0.5 kcal/mol for each substitution. Thus, increased substitution to the α-carbon stabilizes the reactant alkene, destabilizes the transition state due to sterics, and has little effect on the product stability, so substitution increases the activation energy and the reaction enthalpy – hence, a positive slope.

Rate Rules for Vinyl + Alkenes: Arrhenius Parameterization

A modified-Arrhenius fit for both the experimental values and the transition state calculations are shown in Table 14. For addition to the unsubstituted carbon in iso-butene, the transition-state rate constant is slightly higher than the measured rate constant for temperatures below 350 K. This discrepancy could be due to a small under-prediction in the calculated barrier height, or it could be due to the hindered rotor and tunneling corrections, both of which are more sensitive to low temperature behavior. To correct for this discrepancy, the computed value for the activation energy was increased by 0.2 kcal/mol, and the A-factor adjusted accordingly. With this minor correction, the addition to the α-carbon of iso-butene correctly matches the experimental values. At those low temperatures, the two competing channels will be negligible.

To determine the temperature exponent for the rate expression, the exponential pre-factor for the transition-state theory rate constant was fit to an equation of the form

$$A\left(\frac{T}{1000\ [\mathrm{K}]}\right)^{n} = \kappa(T)\frac{k_B T}{h}\frac{Q_{TS}}{Q_{AB}} \qquad (10)$$

The resulting values for the pre-exponential factor, A, and the temperature exponent, n, are shown in columns 3 and 4, respectively, of Table 14. Between 300 and

700 K, the dominant rate for each vinyl + alkene system is the major addition channel, and the average value of n for these channels is 1.7; thus, to simplify comparison, an average value of n = 1.7 was used for the Arrhenius fits in Table 14.

Rate Rules for Vinyl + Alkenes: Addition

Two approaches for generating rate rules are commonly employed for carbon-centered radical addition to unsaturated hydrocarbons. One approach is to the curve-crossing model or state correlation diagram, which is the method used by Fischer and Radom[23] and by Henry et al.[24]. The other approach is group additivity, which is used by Sabbe et al.[25]. Each method will be applied to the reaction of vinyl radical with alkenes below.

In the curve-crossing model, it is assumed that the activation energy can be fit to an Evans-Polanyi expression, multiplied by a polar correction factor:

$$E_a = \left(E_a^0 + \alpha \Delta H_{298K}\right) F_n F_e \tag{11}$$

where the terms F_n and F_e are nucleophilic and electrophilic correction factors, respectively. The expression for the electrophilic correction factor is given by:

$$F_e = 1 - \exp\left[-\left(\left[E_{ip}(A) - E_{ea}(R) - C_e\right]/\gamma_e\right)^2\right] \tag{12}$$

where E_{ip} is the ionization energy, E_{ea} is the electron affinity, R is the radical, A is the alkene, C_e is the Coulomb attraction, and γ_e is the strength of the interaction. The ionization energy and electron affinity are calculated below. The parameters E_a^0, α, C_e, and γ_e are usually adjusted to fit the data. For reactions that exhibit strong electrophilic polar effects, the nucleophilic correction factor is assumed to be unity[23]. According to

this model, strong electrophilic polar effects are sufficient to cause a negative slope in an Evans-Polanyi plot. To utilize this method properly, one must calculate the electronic energies for the ionic species. The final step of the G3 method in Gaussian03 failed to converge for some of the ionic species, so these results could not be compared to the G3 energies for the neutral species. Instead, coupled cluster calculations were used to determine the necessary ionization energies and electron potentials. The neutral species, the cation, and the anion geometries were calculated at the RCCSD(T)/aug-cc-pvtz//RHF/aug-cc-pvdz level theory. These calculations were performed in MOLPRO, and the results, summarized in Table 10, are in excellent agreement with experimental values[27]. The curve-crossing method is typically used for larger data sets which generally exhibit an Evans-Polanyi relation with a positive slope, which as noted above does not describe the current set of reactions. To use this approach, we fixed a slope of $\alpha = 0.2$, which is a comparatively small value, typical for early transition states with low barriers (for comparison, $\alpha = 0.244$ for methyl addition to alkenes, which has a higher activation energy[23]). Figure 10a is a plot of the electrophilic correction factor, F_e, versus the electrophilic polar effect, $E_{ip}(A) - E_{ea}(R)$. The symbols are the result of dividing the E_a's in Table 14 by $(E_a^0 + 0.2 * \Delta H_{298K})$, where E_a^0 as adjusted to provide a good fit, and the solid line is the result of fitting C_e and γ_e in Equation 12 to the data. As seen in the figure, the fit is remarkably good, even noting the model is adjusting three parameters (E_a^0, C_e, and γ_e) to fit four data. The fitted values of E_a^0, C_e, and γ_e are 9.9 kcal/mol, 7.8 eV, and 0.73 eV, respectively. As a result of the excellent fit, the activation energies estimated by using Equation 12 agree with the calculated activation energies in Table 14 to within 0.01 kcal/mol. Despite the strong agreement, there are two disadvantages to

this approach. First, the selection of $\alpha = 0.2$, although reasonable, is somewhat arbitrary; we may be overfitting the data, so there is no guarantee that Equation 12 would work equally well for vinyl addition to unsubstituted carbons in larger alkenes. Second, this method does not work well for addition to substituted carbons. Since the polar correction factor does not account for steric hindrances, a separate Evans-Polanyi relation is required for addition to the substituted end. These results are shown in Figure 10b, which uses the Evans-Polanyi parameters from Figure 9b. The fitted values for C_e, and γ_e are 8.4 eV, and 0.06 eV, respectively. Unlike addition to an unsubstituted carbon, the electrophilic correction factor for addition to a substituted carbon is not monotonically increasing with $E_{ip}(A) - E_{ea}(R)$, which suggests that there is little to be gained by using this method for addition to substituted alkenes. The curve-crossing model predictions for the activation energies are shown in Figure 11a.

It should be noted that the curve-crossing method does not predict A-factors. Consequently, a general A-factor (equivalent to that for vinyl + iso-butene) is suggested: $A = 5.5\times10^{-13}\times(T/1000)^{1.7}$ [cm^3 $molecule^{-1}$ s^{-1}]. The A-factors derived below from the group-additivity approach should not be used in conjunction with the activation energies derived from the curve-crossing method, as these A-factors were optimized with the group-additivity E_a's, and resulting rate constant would be too high.

The group additivity approach is more flexible. In this method, one begins with a rate equation for a reference reaction – here assumed to be vinyl + ethene – and suggests changes to the A-factor and activation energy based upon substitutions to the reference reactants. For each substitution, the A-factor will decrease due to rotational effects, and substitutions that cause steric effects will decrease the A-factor further. Substitutions to

the β-carbon will decrease the activation energy due to increased charge donation, and substitutions made to the α-carbon will increase the barrier due to steric repulsion.

For the addition of the vinyl radical to a double-bonded carbon in a generic alkene:

1. Start with $A = 1.2\times10^{-12}\times(T/1000)^{1.7}$ [cm^3 $molecule^{-1}$ s^{-1}] and $E_a = 3.3$ [kcal/mol].
2. For each substituted group on the α-carbon, decrease A by 0.5×10^{-12} cm^3 $molecule^{-1}$ s^{-1} and increase E_a by 1.0 kcal/mol.
3. For each substituted group added to the β-carbon, decrease A by 0.3×10^{-12} cm^3 $molecule^{-1}$ s^{-1} and decrease E_a by 0.4 kcal/mol.

This rate estimation method is compared to the experimental results in Figure 13, with details at the end of the next section. The group-additivity predictions for the activation energies are shown in Figure 11b.

To compare the curve-crossing method and the group-additivity approach, the rate constant for vinyl + 2-methyl-1-butene was calculated using the same methods described in the Theory section. The modified-Arrhenius parameters are provided in Table 14. As seen in Figure 11a and Figure 11b, the curve-crossing model does a slightly better job of predicting the activation energy, which suggests that it has a firmer theoretical foundation for addition reactions of highly electrophilic radicals. However, the group-additivity approach is still remarkably accurate. Furthermore, the group-additivity approach is considerably simpler, since it requires neither Evans-Polanyi parameters nor ionization potential and electron affinity calculations. The ratio of the calculated rate constant to the predicted rate constant for each method is shown in Figure 12. This figure illustrates

that the calculated rate constant and the group-additivity predicted rate constant agree to within 25% over the entire range of 400 to 2000 K, which suggests there is no need for the more detailed calculations required by the curve-crossing method.

Rate Rules for Vinyl + Alkenes: H-abstraction

As mentioned previously, the vinyl radical can abstract an H-atom from the alkene. For ethene, the result is a symmetric reaction, so it is not considered here. For the other four alkenes studied, the lowest barrier to abstraction is when the alkene becomes a resonantly stabilized (allylic) radical: propene to allyl, 1-butene and 2-butene to 1-methyl-allyl, and iso-butene to 2-methyl-allyl. Although it is possible for vinyl to abstract other H-atoms, the barriers are significantly higher: for vinyl + propene, the barriers to abstract an H-atom from C1 or C2 are roughly 6 and 4 kcal/mol higher, respectively, and for vinyl + 1-butene, the barrier to abstract an H-atom from the methyl group is 5 kcal/mol higher. The Arrhenius parameters for these calculations are shown in Table 15. Comparing the rates for addition and H-abstraction, it is clear that the addition rates have lower barriers, and that the abstraction rate A-factors have higher temperature-dependencies. Thus, at higher temperatures, the abstraction rates will dominate the addition rate, consistent with entropic intuition.

To generate a rate rule for H-abstraction, it is customary to divide by the number of H-atoms that, when abstracted, will yield identical products. For 1-butene, the H-atom comes from the CH_2 group on carbon C3; for the other three alkenes, the H-atoms belong to methyl groups. Thus, propene is normalized by three, 1-butene by two, and 2-butene and isobutene by six. When normalized in this regard, the rates for abstraction from a

methyl group are remarkably consistent, as shown in the last two columns of Table 15. The abstraction rate from propene has a slightly higher A-factor, consistent with the high rotational constant for propene, and it also has a slightly higher barrier. The rate for abstraction from 1-butene is roughly a factor of five faster between 500 and 2000 K, as expected, since it is easier to form a secondary radical than a primary radical. Based upon the rates presented in Table 15, a generic rule for vinyl H-abstraction is:

For abstraction from CH_3:

$A = 2.7\times10^{-13}\times(T/1000)^{2.8}$ cm^3 molecule^{-1} s^{-1} and $E_a = 5.4$ kcal/mol

Of course, one must remember to multiply this rate coefficient by the number of equivalent H atoms (i.e. 3 for each methyl group adjacent to the double-bond group). For abstraction from CH_2:

$A = 5.6\times10^{-13}\times (T/1000)^{2.8}$ cm^3 molecule^{-1} s^{-1} and $E_a = 4.1$ kcal/mol

Again, one must remember to multiply this rate coefficient by the number of equivalent H atoms (i.e. 2 for each CH_2 groups adjacent to the double-bond group).

This rate rule agrees very well with the rate coefficients computed from quantum chemistry. From 400 to 850 K, the agreement is within a factor of 2, and from 850 to 2000 K, the agreement is within 25%.

Rate Rules for Vinyl + Alkenes: Application

Although the major addition channel is the dominant reaction in the experimental temperature range, the H-abstraction channel is not negligible. Indeed, for 1-butene and iso-butene, it can be as much as 25% of the total rate, and even more at combustion-relevant temperatures. Consequently, it is important to include both addition and abstraction reactions when comparing the effectiveness of the new rate rule with the

experimental data. The group additivity rate rules for addition and H-abstraction were applied for the five alkenes. The experimentally observed rate coefficients divided by the rate coefficients obtained from the rate rules are plotted versus the temperature in Figure 13. With the exception of 2-butene at low temperatures, the rate rules agree with the experimental data to within 40%.

Conclusions

The reaction kinetics and product channels of the various $C_2H_3 + C_4H_8$ reactions have been studied at temperatures ranging from 300 to 700 K and at a pressure of 100 Torr. A weighted Arrhenius fit to the experimental rate coefficients yields for 1-butene, 2-butene and iso-butene respectively:

$$k_1 = (1.3\pm0.3)\times 10^{-12}\ \text{cm}^3\ \text{molecules}^{-1}\ \text{s}^{-1}\ \exp[-(2200 \pm 120)\ \text{K/T}] \quad (9)$$

$$k_2 = (1.7\pm0.3)\times 10^{-12}\ \text{cm}^3\ \text{molecules}^{-1}\ \text{s}^{-1}\ \exp[-(2610 \pm 120)\ \text{K/T}] \quad (10)$$

$$k_3 = (1.0\pm0.1)\times 10^{-12}\ \text{cm}^3\ \text{molecules}^{-1}\ \text{s}^{-1}\ \exp[-(2130 \pm 50)\ \text{K/T}] \quad (11)$$

RRKM/ME calculations based on G3 characterization of the C_6H_{11} potential energy surface are presented, and are in excellent agreement with the experimental data. These calculations indicate that at low temperatures, the dominant product for each system will be the collisionally stabilized initial adducts, 5-hexen-3-yl, 2-ethyl-3-buten-1-yl, and 2-ethyl-cyclopropylmethyl for 1-butene; 3-methyl-4-penten-2-yl and 2,3-dimethyl-cyclopropylmethyl for 2-butene; and 2-methyl-4-penten-2-yl, 2,2-dimethyl-3-buten-1-yl, and 2,2-dimethyl-cyclopropylmethyl for iso-butene. At higher temperatures, the addition-isomerization-dissociation channels will yield a mixture of dienes, H atoms, and alkyl radicals, and the direct H-abstraction channels will yield ethene plus methyl-allyl.

Although several cyclic species are energetically accessible, the yield of cyclic products (with the exception of the cyclopropylmethyl isomers formed via equilibration with the initial adducts) is negligible under the (T,P) conditions considered. The experimental activation energies for the addition reactions do not vary monotonically with ΔH_{rxn}; instead they scale with electrophilicity and steric effects consistent with the present and prior quantum chemical calculations. A new group-additivity based rate rule has been provided for the addition reactions and H-abstraction reaction for the vinyl radical with generic alkenes. This rate rule is in excellent agreement with both the available experimental data and quantum chemical calculations.

Acknowledgments

This work is supported by Division of Chemical Sciences, Geosciences, and Biosciences, the Office of Basic Energy Science (BES) of the U.S. Department of Energy (DOE) through contract DE-FG02-98ER14914. We are very grateful to Stephen Klippenstein for allowing us to use the new version of VariFlex prior to its general release, and for his many helpful comments and suggestions. We are also grateful to Professor Robert W. Field for lending us the Nd:YAG photolysis laser used in the experiments. Special thanks are given to Sandeep Sharma, Adam Steeves, and Paul Abel for their useful discussions. The probe laser system used in these experiments was provided by the George Harrison Spectroscopy Laboratory, with financial support from the National Science Foundation. CFG gratefully acknowledges fellowship support from the Dept. of Defense and the NSF.

Supporting Information Available

Predicted rates of vinyl radical plus ethene, propene, 1-butene, 2-butene, and iso-butene to each of the major product channels in various pressures of N2 and various temperatures, including files in CHEMKIN format. Also, the computed geometrical structures and energies of the transition states (saddle points). This information is available free of charge via the Internet at http://pubs.acs.org.

Figure Captions

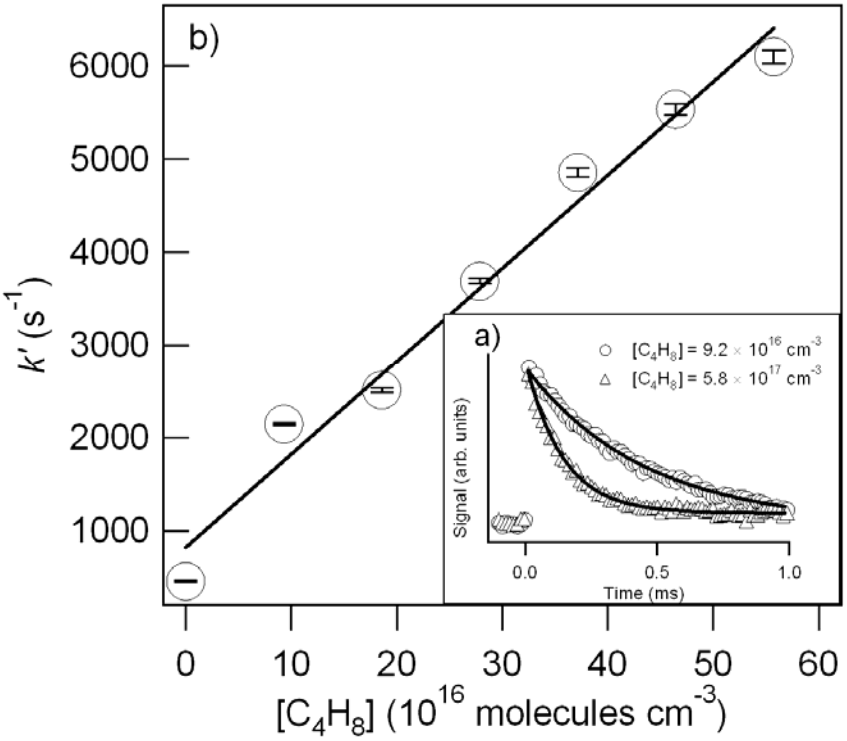

Figure 1: (**a**) Recorded decay of C_2H_3 at 700 K and 100 Torr for the conditions [1-C_4H_8] = 9.2×10^{16} molecules cm^{-3} (circles) and [1-C_4H_8] = 5.8×10^{17} molecules cm^{-3} (triangles). Every 700^{th} point is shown for clarity. **b**) Pseudo-first-order C_2H_3 decay rate k′ vs. [1-C_4H_8], at a temperature of 400 K and a pressure of 100 Torr.

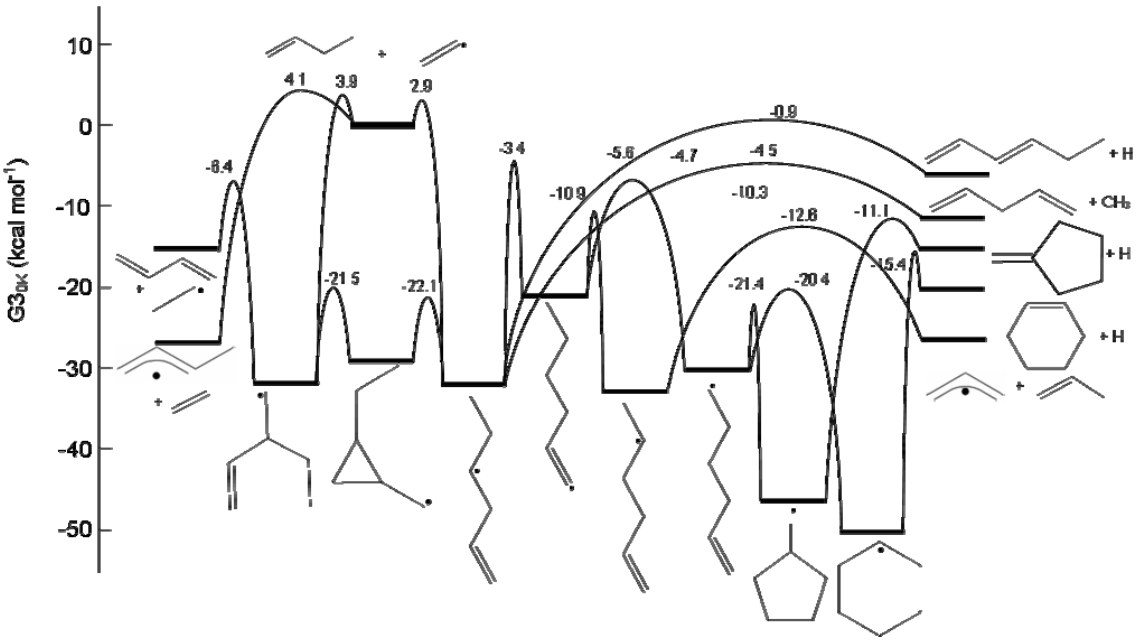

Figure 2: PES for the vinyl + 1-butene system.

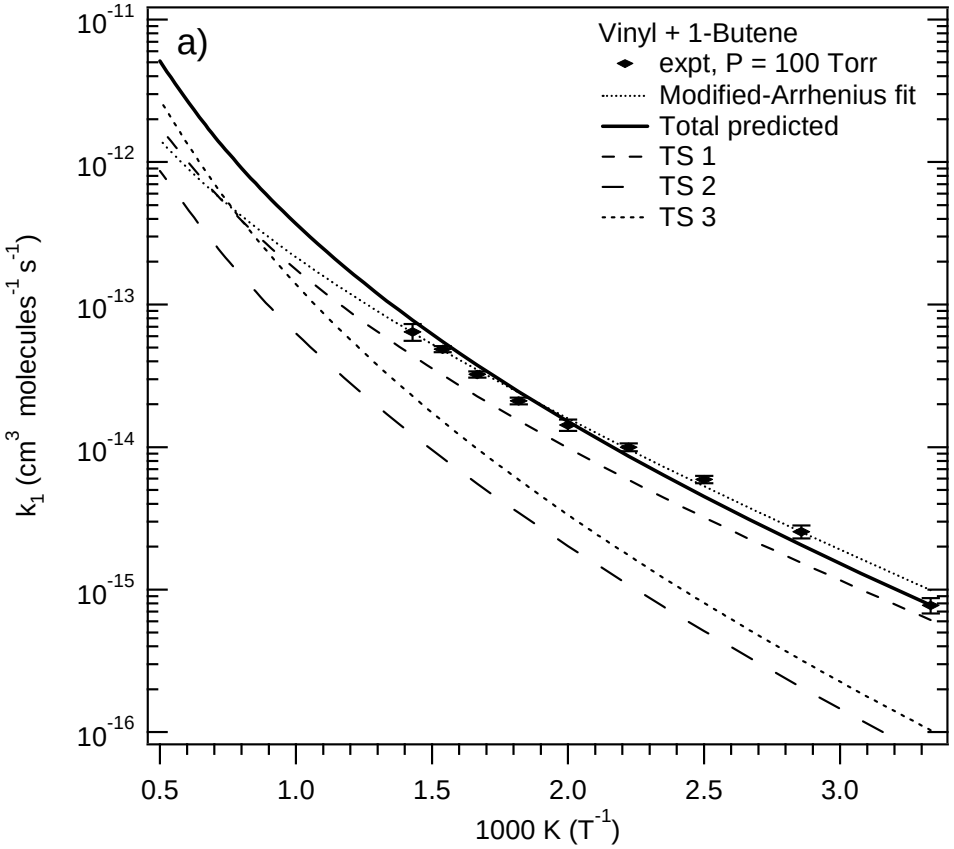
a)
Vinyl + 1-Butene
expt, P = 100 Torr
Modified-Arrhenius fit
Total predicted
TS 1
TS 2
TS 3
k_1 (cm^3 $molecules^{-1}$ s^{-1})
1000 K (T^{-1})

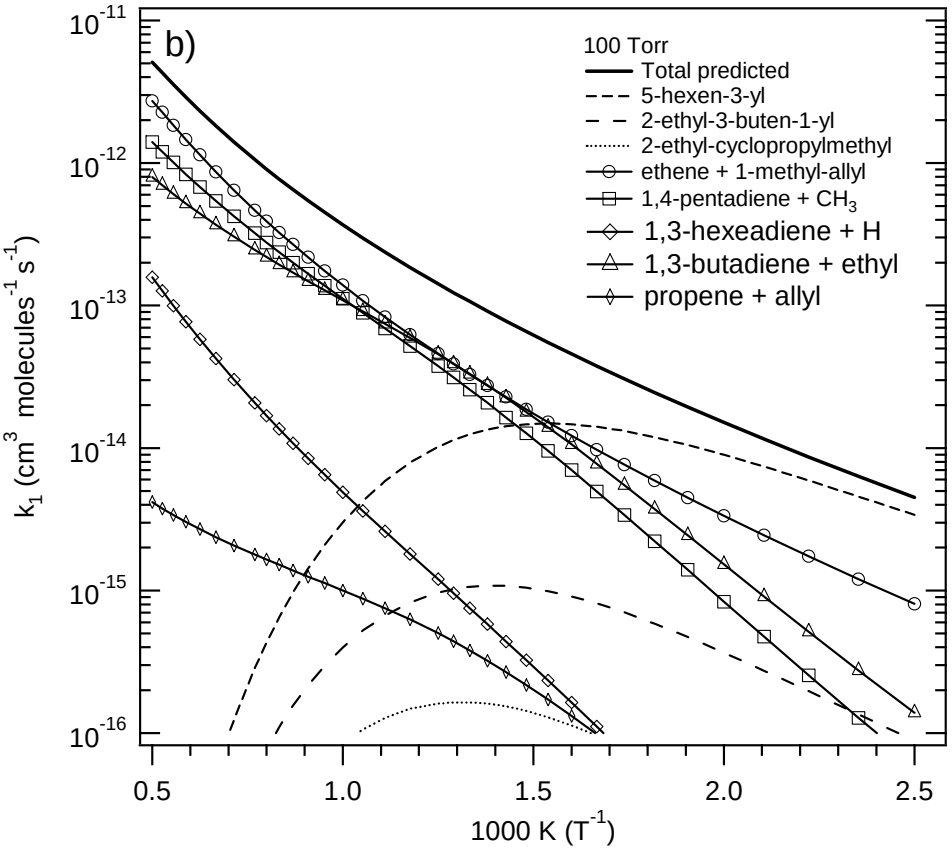
b)
100 Torr
Total predicted
5-hexen-3-yl
2-ethyl-3-buten-1-yl
2-ethyl-cyclopropylmethyl
ethene + 1-methyl-allyl
1,4-pentadiene + CH_3
1,3-hexeadiene + H
1,3-butadiene + ethyl
propene + allyl
k_1 (cm^3 $molecules^{-1}$ s^{-1})
1000 K (T^{-1})

Figure 3: a) Temperature dependence of the total rate constant of the reaction of vinyl with 1-butene. The total high-pressure limit rate coefficent is shown as the thick solid line; the dashed lines show the rate constants through each entrance channel. **b**) Master equation predictions for the product channels of the reaction between vinyl radical and 1-butene in 100 Torr of He. The dashed lines are the rates coefficients for collisional stabilization of the initial adducts; the lines with symbols are chemically-activated bi-molecular products; the solid line is the total rate coefficient.

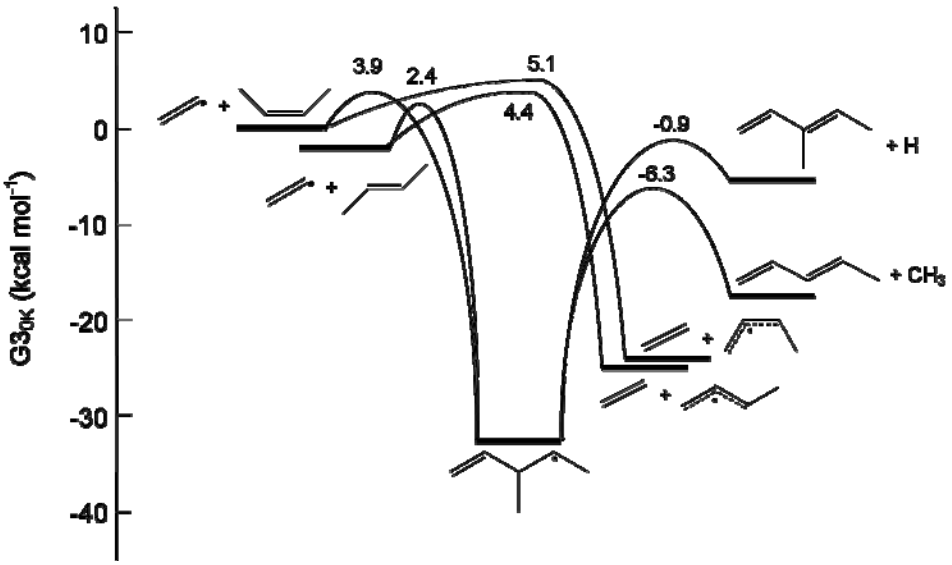

Figure 4: Simplified PES for the vinyl + 2-butene system.

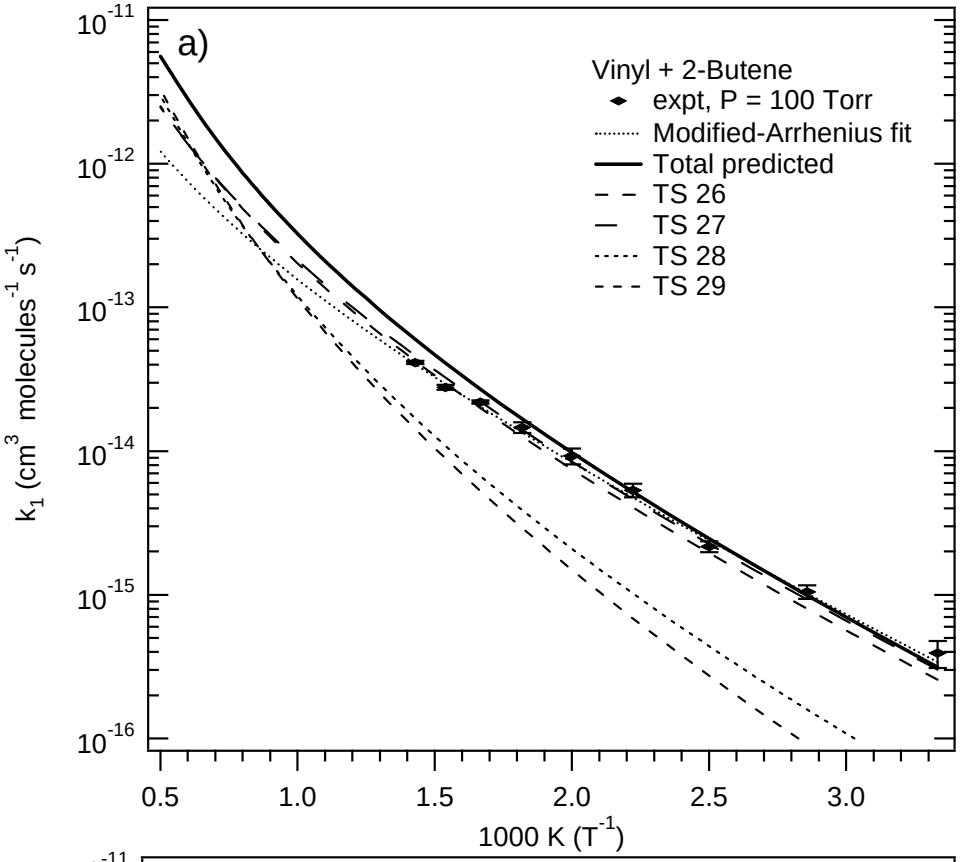
a)
Vinyl + 2-Butene
expt, P = 100 Torr
Modified-Arrhenius fit
Total predicted
TS 26
TS 27
TS 28
TS 29
k_1 (cm^3 $molecules^{-1}$ s^{-1})
1000 K (T^{-1})

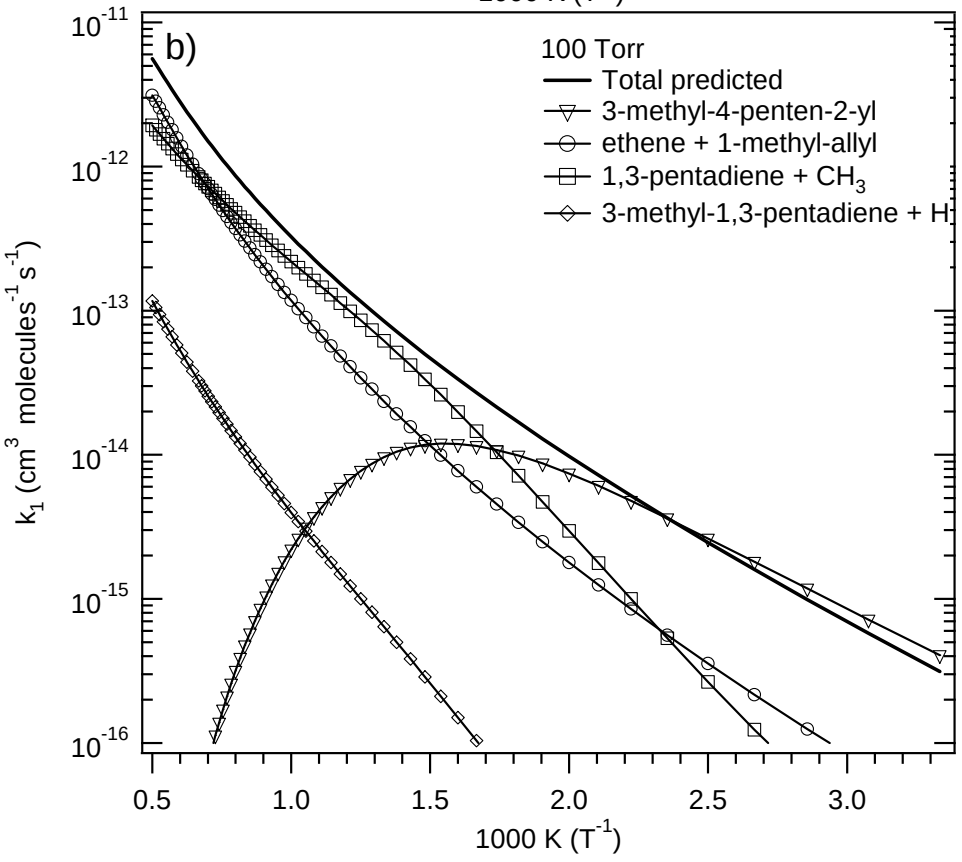
b)
100 Torr
Total predicted
3-methyl-4-penten-2-yl
ethene + 1-methyl-allyl
1,3-pentadiene + CH_3
3-methyl-1,3-pentadiene + H
k_1 (cm^3 $molecules^{-1}$ s^{-1})
1000 K (T^{-1})

Figure 5: a) Temperature dependence of the total rate coefficient of the reaction of vinyl with 2-butene. The total high-pressure limit rate constant is shown as the thick solid line, and the various entrance channels are shown as the dashed lines. b) Master equation predictions for the product channels of the reaction between vinyl radical and 2-butene in 100 Torr of He. Both (a) and (b) assume a 50/50 blend of cis- and trans-2-butene.

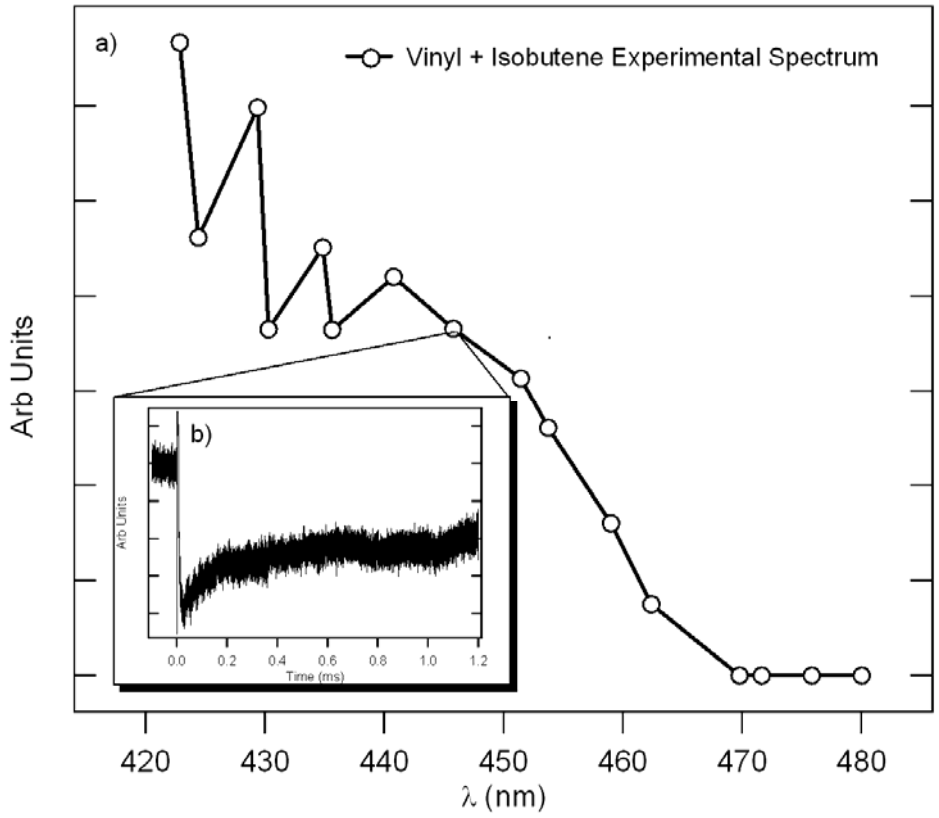

Figure 6: a) Low resolution spectrum of the background signal observed in the vinyl + isobutene system, T = 700 K, P_{He} = 100 Torr. The spectrum is taken at 0.8 ms. To avoid this interference, k_3 was measured at 475 nm. b) Transient absorption measured at 423 nm. The background signal lasts for ~5 ms, before returning to baseline; it is attributed to 2-methyl-allyl radical.

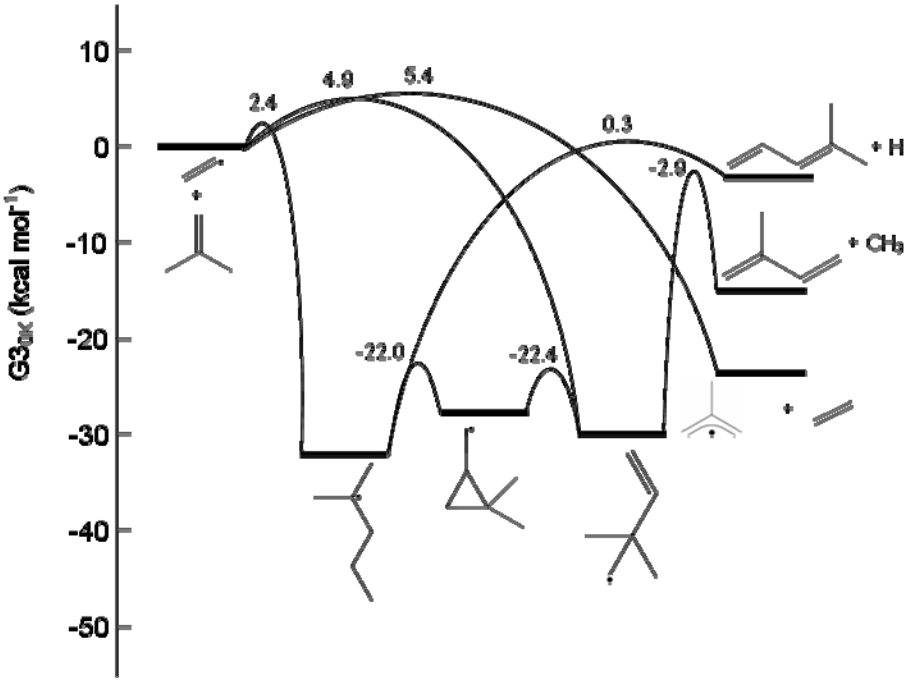

Figure 7: Simplified PES for the vinyl + iso-butene system.

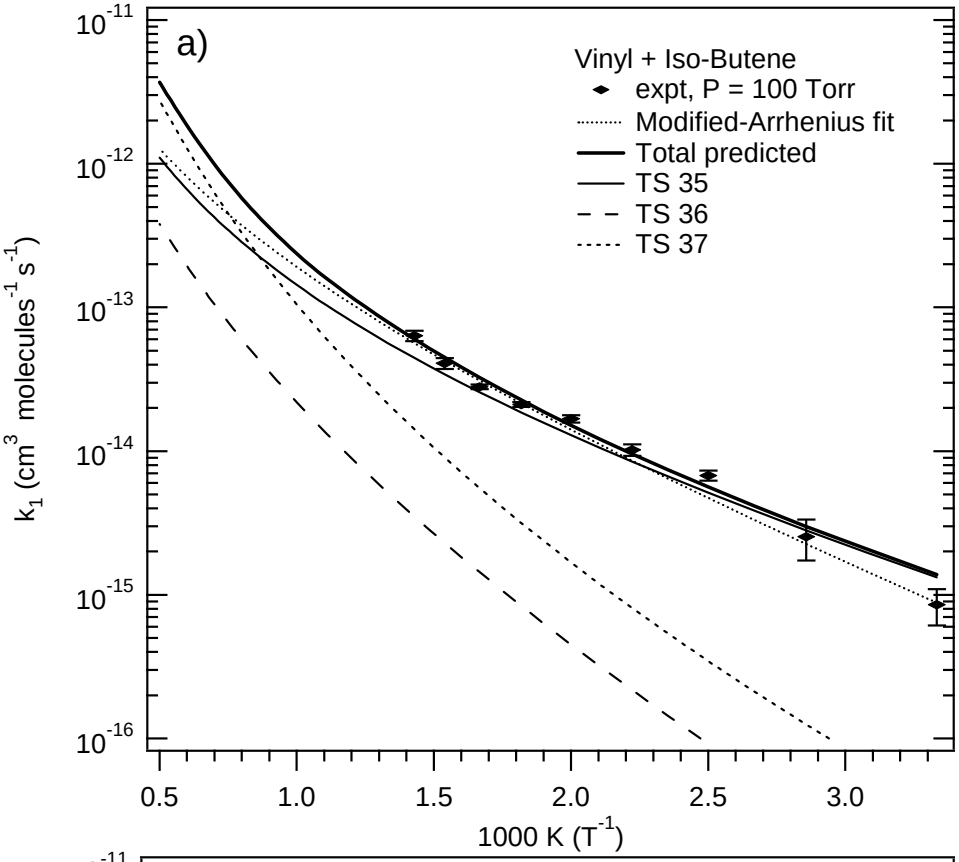
a)
Vinyl + Iso-Butene
expt, P = 100 Torr
Modified-Arrhenius fit
Total predicted
TS 35
TS 36
TS 37
k_1 (cm^3 $molecules^{-1}$ s^{-1})
1000 K (T^{-1})

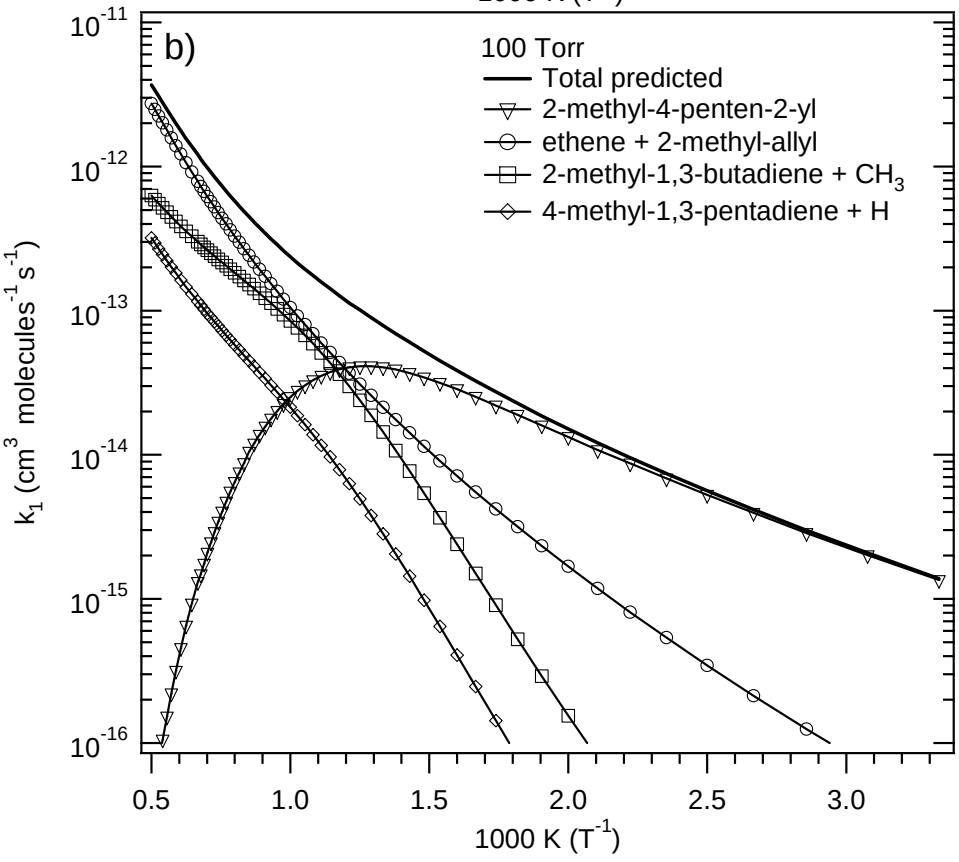
b)
100 Torr
Total predicted
2-methyl-4-penten-2-yl
ethene + 2-methyl-allyl
2-methyl-1,3-butadiene + CH_3
4-methyl-1,3-pentadiene + H
k_1 (cm^3 $molecules^{-1}$ s^{-1})
1000 K (T^{-1})

Figure 8: a) Temperature dependence of the total rate constant of the reaction of vinyl with iso-butene. The high-pressure limit rate constant is shown as the solid line. The rate constants through the different entrance channels are shown as the dashed lines. **b**) Master equation predictions for the product channels of the reaction between vinyl radical and 2-butene in 100 Torr of He.

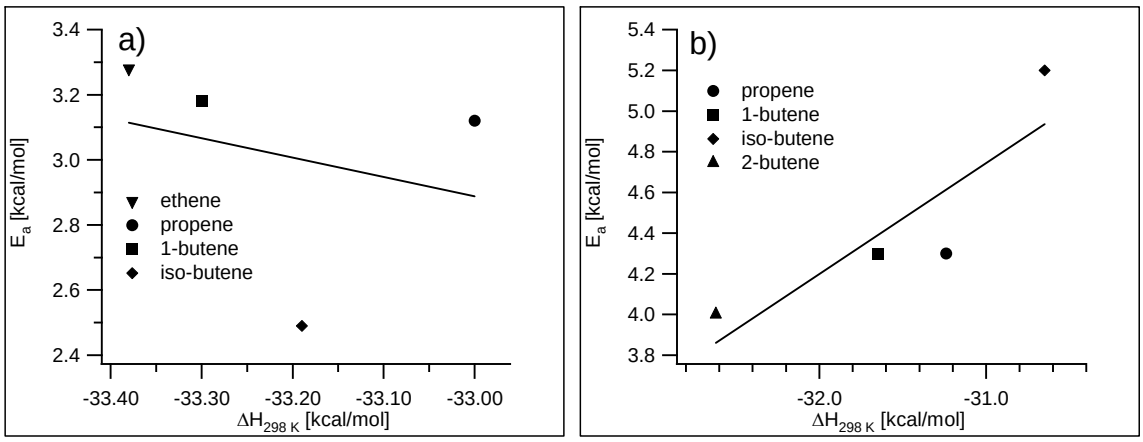

Figure 9: Evans-Polanyi plot for vinyl + alkenes. a) The data are the calculated activation energies for addition the unsubstituted end of the alkene, and the solid line is the least-squares straight-line fit, given by E_a = -16.71 (±49.1) - 0.59 (±1.48) ΔH_{298}. b) The data are the calculated activation energies for addition to the substituted end of the alkene, and the solid line is the least-squares straight-line fit, given by E_a = 21.67 (±6.88) + 0.54 (±0.22) ΔH_{298}.

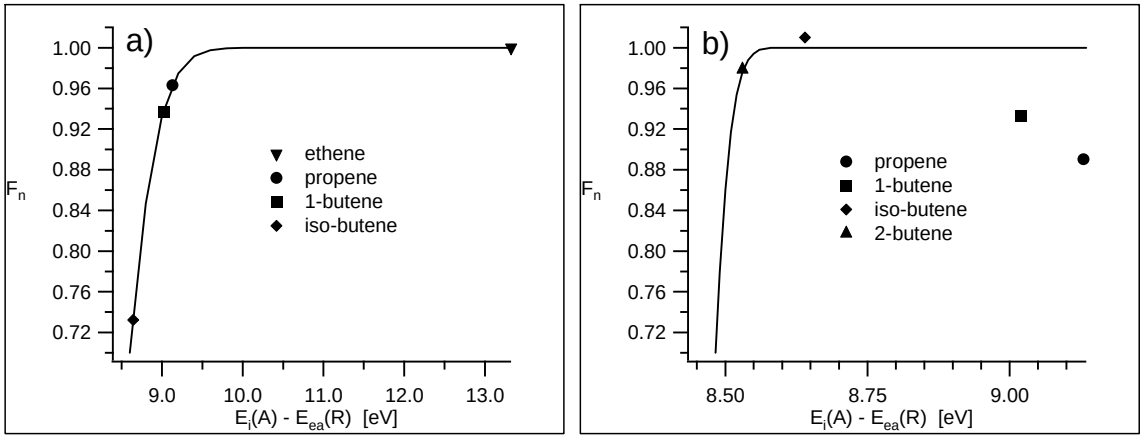

Figure 10: Electrophilic polar correction for vinyl addition to alkenes. a) Addition to the unsubstituted carbon: The data are the activation energies from Table 14 divided by the Evans-Polanyi relation: Ea = 9.9 + 0.2 ΔH_{298K}. The solid line is the fit from Equation 12, with C_e = 7.8 eV and γ_e = 0.73 eV. b) Addition to the substituted carbon: The data are the activation energies from Table 14 divided by the Evans-Polanyi relation: Ea = 21.7 + 0.5 ΔH_{298K}. The solid line is the fit from Equation 12, with C_e = 8.4 eV and γ_e = 0.06 eV.

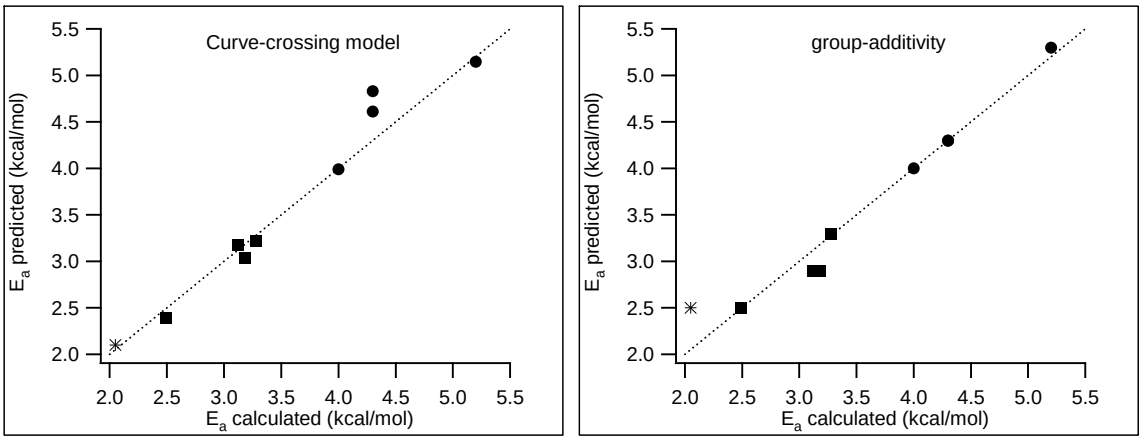

Figure 11: Rate rule activation energies. a) The activation energies predicted by the curve-crossing method. b) The activation energies predicted by the group-additivity method. In both plots, the x-axis is the activation energies from Table 14. The squares are addition to the unsubstituted carbon, the circles are addition to the substituted carbon, and the star is the value for vinyl + 2-methyl-1-butene. The curve-crossing method predicts the activation energy for the test reaction, vinyl + 2-methyl-1-butene, with greater accuracy (agreement within 0.1 kcal/mol).

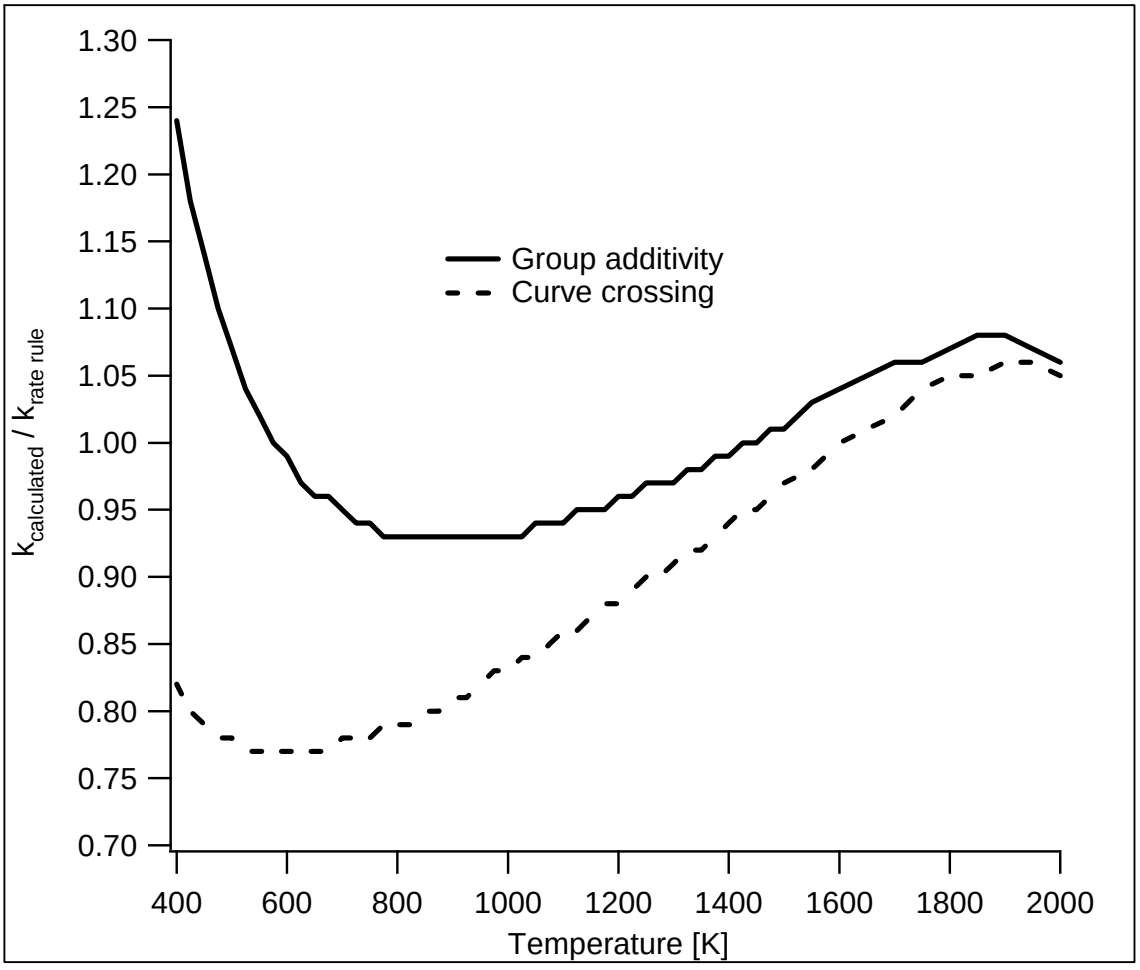

Figure 12: Rate rules vs. calculated rate for vinyl + 2-methyl-1-butene. For both methods, the calculated rate constant is divided by the rate constant predicted by the rate rule. The solid line is the rate

coefficient predicted by the group-additivity method, and the dashed line is the rate coefficient predicted by the curve-crossing method. The curve-crossing method used the A-factor of $A = 5.5\times10^{-13}\times(T/1000)^{1.7}$ [cm^3 $molecule^{-1}$ s^{-1}], which is equivalent to the A-factor of vinyl addition to the unsubstituted end of iso-butene.

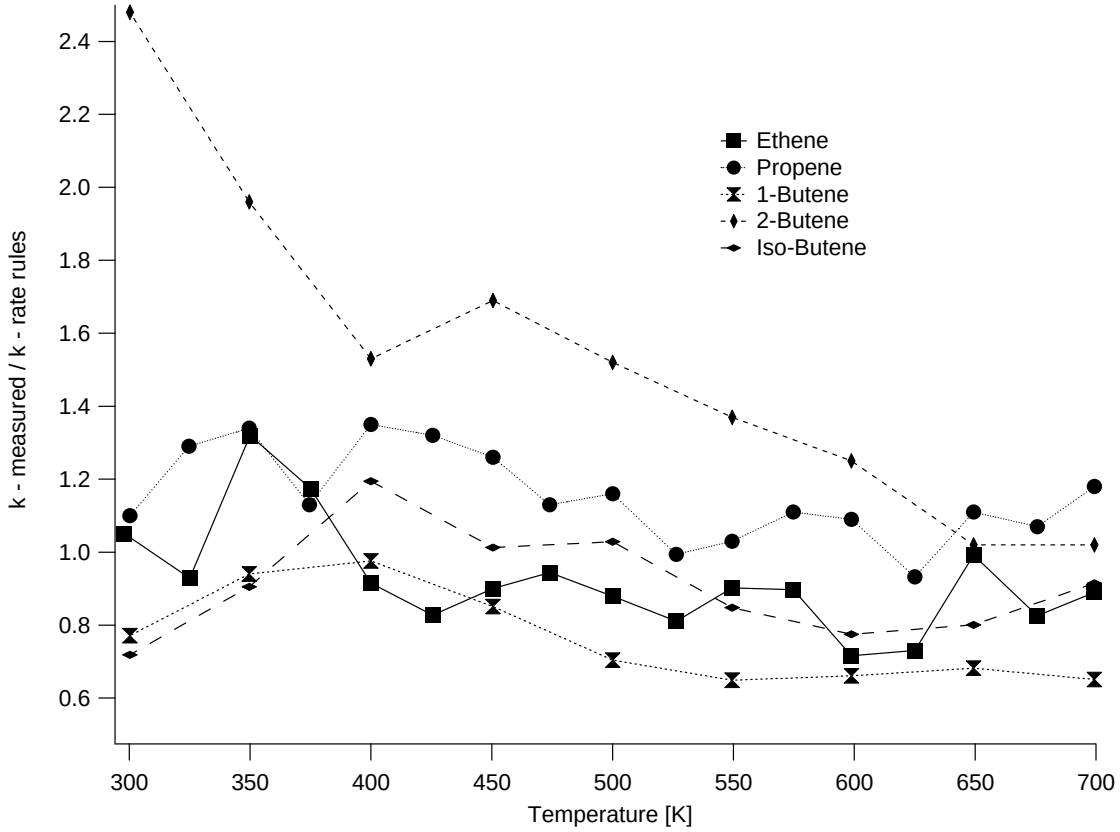

Figure 13 Rate Rule versus Experimental Data. The dots are the experimental data for vinyl + alkenes divided by the rate rule prediction (sum of the two addition channels plus H-abstraction channel).

Tables

.

T, (K)	P (Torr)	$[C_2H_3I]$ (10^{14} cm^{-3})	$[C_2H_3]_0$[a] (10^{12} cm^{-3})	[1-butene] (10^{17} cm^{-3})	k_1[b] (10^{-15} cm^3 molecule^{-1} s^{-1})	k_1' (s^{-1})
292	100	5.5	7.5	2.2 – 18.1	0.8 ± 0.1	740
350	100	5.5	7.4	1.8 – 10.9	2.6 ± 0.3	600
400	100	5.6	4.9	0.9 – 6.5	5.90 ± 0.4	560
450	100	4.6	5.2	0.9 – 5.6	10.0 ± 0.7	460
500	100	4.6	3.2	0.5 – 3.7	14.3 ± 1.3	310
550	100	4.6	3.6	0.5 – 3.2	21.1 ± 1.1	450
600	100	4.6	3.6	0.2 – 2.3	32.4 ± 1.7	450
650	100	4.6	4.5	0.2 – 2.3	48.6 ± 2.4	330
700	100	4.6	2.9	0.2 – 1.8	64.6 ± 8.6	360

Table 1 Conditions and Results of Experiments to Measure k_1 (vinyl + 1-butene)

[a] Determined using C_2H_3 cross section of 2×10^{-19} cm^2 at 423.2 nm[28]
[b] Uncertainty limits (± 1σ) based on statistical uncertainties in the fits.

T, (K)	P (Torr)	$[C_2H_3I]$ (10^{14} cm^{-3})	$[C_2H_3]_0$[a] (10^{12} cm^{-3})	[2-butene] (10^{17} cm^{-3})	k_2[b] (10^{-15} cm^3 molecule^{-1} s^{-1})	k_2' (s^{-1})
292	100	5.5	9.8	2.7 – 19.2	0.4 ± 0.1	730
350	100	5.5	8.7	1.8 – 10.9	1.1 ± 0.1	700
400	100	5.6	6.90	1.4 – 8.3	2.2 ± 0.2	520
450	100	4.6	5.1	0.9 – 7.4	5.3 ± 0.6	910
500	100	4.6	4.4	0.9 – 4.6	9.3 ± 1.2	730
550	100	4.6	4.5	0.7 – 4.1	14.6 ± 1.3	710
600	100	4.6	3.6	0.7 – 4.1	21.9 ± 0.6	780
650	100	4.6	3.6	0.5 – 2.7	27.8 ± 1.1	380
700	100	4.6	4.5	0.5 – 3.2	41.4 ± 1.1	630

Table 2 Conditions and Results of Experiments to Measure k_2 (vinyl + 2-butene).

[a] Determined using C_2H_3 cross section of 2×10^{-19} cm^2 at 423.2 nm[28]
[b] Uncertainty limits (± 1σ) based on statistical uncertainties in the fits.

T, (K)	P (Torr)	$[C_2H_3I]$ (10^{15} cm^{-3})	$[C_2H_3]_0$[a] (10^{13} cm^{-3})	[iso-butene] (10^{17} cm^{-3})	k_3[b] (10^{-15} cm^3 molecule^{-1} s^{-1})	k_3' (s^{-1})
292	100	1.6	1.3	2.1 – 10.1	0.9 ± 0.1	650
350	100	1.7	1.3	3.2 – 9.8	2.5 ± 0.8	500
400	100	1.9	1.3	1.4 – 8.3	6.8 ± 0.6	590
450	100	1.9	1.3	0.9 – 5.2	10.2 ± 1.0	590
500	100	1.8	1.6	0.9 – 5.0	16.8 ± 1.0	820
550	100	2.3	1.1	0.4 – 3.6	21.1 ± 0.8	760
600	100	1.8	0.6	0.6 – 4.8	28.0 ± 1.0	460
650	100	1.8	0.6	0.2 – 2.3	40.8 ± 3.5	680
700	100	1.8	0.6	0.2 – 2.3	63.5 ± 5.2	390

Table 3 Conditions and Results of Experiments to Measure k_3 (vinyl + iso-butene).

[a] Determined using C_2H_3 cross section of ~5.0×10^{-20} cm^2 at 472.0 nm[28]

[b] Uncertainty limits (± 1σ) based on statistical uncertainties in the fits.

#	species name	Structure	G3 ΔE_0^0 (kcal/mole)
R1	vinyl + 1-butene		0.00
W1	5-hexen-3-yl	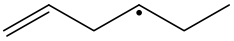	-32.4
W2	1-hexen-1-yl	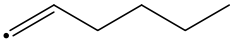	-21.1
W3	5-hexen-2-yl	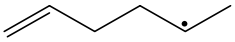	-32.9
W4	1-hexen-2-yl	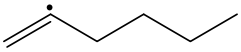	-24.5
W5	5-hexen-1-yl	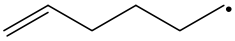	-30.8
W6	Cyclohexyl	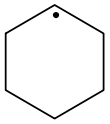	-50.5
W7	2-ethyl-cyclopropylmethyl	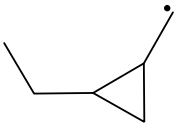	-29.7
W8	2-ethyl-3-buten-1-yl	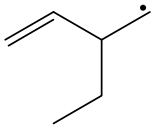	-31.0
W9	1-propyl-allyl	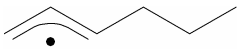	-47.7
W10	1-methyl-1-ethyl-allyl	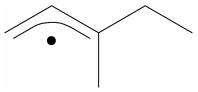	-50.6
W11	Cyclopentylmethyl	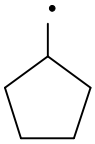	-44.5
P1	1,4-pentadiene + methyl	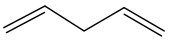 + CH_3	-11.8
P2	propene + allyl	 + 	-26.0
P3	cyclohexene + H	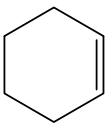 + H	-18.3
P4	1,3-butadiene + ethyl	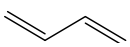 + 	-15.3
P5	ethene + 1-methyl-allyl	 + 	-26.2
P6	1,3-hexadiene + H	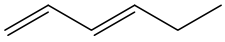 + H	-4.7

P7	2-ethyl-1,3-butadiene + H	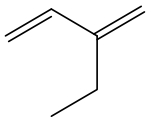	+	H	-4.5
P8	Methylene-cyclopentane + H	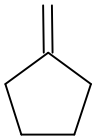	+	H	-14.9

Table 4: Species for vinyl + 1-butene Potential Energy Surface. Note that minor byproducts W9, W10, P6, and P7 are not included in the k(T,P) calculations.

#	reaction	relative energy (kcal/mol)	#	reaction	G3 ΔE_0^0 (kcal/mol)
TS 1	R1 to W1	2.9	TS 16	W6 to P3	-15.4
TS 2	R1 to W8	3.9	TS 17	W11 to P8	-11.1
TS 3	R1 to P5	4.1	TS 18	W8 to P4	-6.4
TS 4	W1 to W2	-3.4	TS 19	W1 to W9	0.2
TS 5	W2 to W3	-10.9	TS 20	W8 to W10	-2.2
TS 6	W2 to W5	-5.6	TS 21	W1 to W3	6.5
TS 7	W3 to W4	-4.7	TS 22	W1 to W4	16.9
TS 8	W4 to W5	-10.3	TS 23	W1 to W5	8.5
TS 9	W5 to W6	-20.4	TS 24	W2 to W4	23.5
TS 10	W5 to W11	-21.4	TS 25	W3 to W5	7.8
TS 11	W1 to W7	-22.1	TS 26	W8 to P7	1.1
TS 12	W7 to W8	-21.5			
TS 13	W1 to P1	-4.5			
TS 14	W1 to P6	-0.9			
TS 15	W3 to P2	-12.6			

Table 5: Transition States for vinyl + 1-butene Potential Energy Surface. Note that TS 19-26 are not included in the final k(T,P) calculations. Energies are relative to vinyl + 1-butene.

#	species name	Structure	G3 ΔE_0^0 (kcal/mole)
R2a	vinyl + cis-2-butene	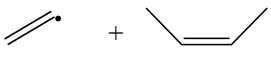	0.0
R2b	vinyl + trans-2-butene	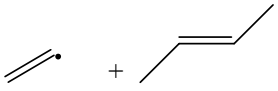	-1.3

W12	3-methyl-4-penten-2-yl	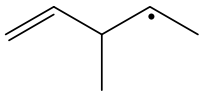			-33.4
W13	1-methyl-1-ethyl-allyl	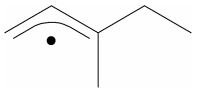			-49.2
P9	1,3-pentadiene + methyl	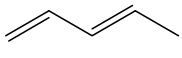	+	CH_3	-17.1
P10	3-methyl-1,3-pentadiene + H	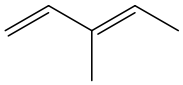	+	H	-5.3
P11a	ethene + cis-1-methyl-allyl	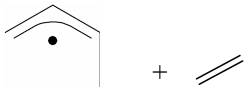	+		-24.2
P11b	ethene + trans-1-methyl-allyl		+		-24.8
P12	3-methyl-1,4-pentadiene + H	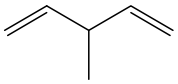	+	H	1.8

Table 6: Species for vinyl + 2-butene Potential Energy Surface. All values are relative to vinyl + cis-2-butene.

#	reaction	G3 ΔE_0^0 (kcal/mol)
TS 27	R2a to W12	3.9
TS 28	R2b to W12	2.4
TS 29	R2a to P11a	5.2
TS 30	R2b to P11b	4.4
TS 31	W12 to W13	0.2
TS 32	W12 to P9	-6.3
TS 33	W12 to P10	-0.9
TS 34	W12 to P12	3.2

Table 7: Transition States for vinyl + 2-butene Potential Energy Surface. All values are relative to vinyl + cis-2-butene. Note that TS 31 and TS 34 were not included in the master equation calculation.

#	species name	Structure			G3 ΔE_0^0 (kcal/mole)
R3	vinyl + iso-butene	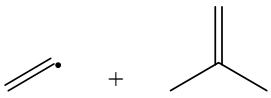	+		0.00
W14	2-methyl-4-penten-2-yl	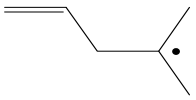			-32.0

W15	2,2-dimethyl-cyclopropylmethyl	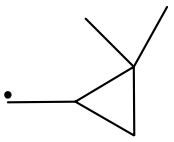			-28.2
W16	2,2-dimethyl-3-buten-1-yl	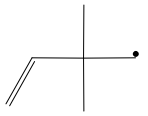			-29.9
W17	isopropyl-allyl	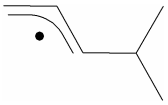			-45.2
P13	4-methyl-1,3-pentadiene + H	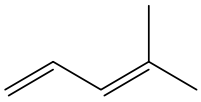	+	H	-3.5
P14	2-methyl-1,3-butadiene + methyl	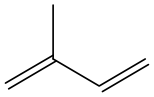	+	CH_3	-14.8
P15	ethene + 2-methyl-allyl	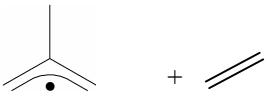	+		-21.9

Table 8: Species for vinyl + iso-butene Potential Energy Surface.

#	reaction	G3 ΔE_0^0 (kcal/mol)
TS 35	R3 to W14	2.4
TS 36	R3 to W16	4.9
TS 37	R3 to P15	5.4
TS 38	W14 to W15	-22.0
TS 39	W15 to W16	-22.4
TS 40	W14 to W17	1.1
TS 41	W14 to P13	0.3
TS 42	W16 to P14	-2.3

Table 9: Transition States for vinyl + iso-butene Potential Energy Surface. Note that TS 40 was not included in the master equation calculation. Energies are relative to vinyl + iso-butene.

	HOMO	SOMO	LUMO	Ionization potential	Electron affinity
Vinyl	-0.5824	-0.425	0.0317	8.67	0.64
Ethene	-0.3794		0.0924	13.96	-0.72
Propene	-0.361		0.0315	9.77	-0.65
1-butene	-0.3604		0.0316	9.66	-0.64
c-2-butene	-0.3441		0.0311	9.17	-0.87
t-2-butene	-0.3443		0.0320	9.17	-0.82
iso-butene	-0.3484		0.0304	9.28	-0.58
2-methyl-1-butene	-0.3478		0.0306	9.17	-0.80

Table 10: Molecular Orbitals and Polar Effects for reactants. The molecular orbital energies (in Hartree/Particle) were taken from RHF/aug-cc-pvtz//RHF/aug-cc-pvdz calculations. The ionization potentials and electron affinities, both in eV, were calculated at the CCSD(T)aug-cc-pvtz//RHF/aug-cc-pvdz level theory.

	Vinyl addition to unsubstituted α-carbon			Vinyl addition to substituted center		
	E_0	ΔH_0	ΔH_{298}	E_0	ΔH_0	ΔH_{298}
Ethene	3.7	-32.5	-33.4			
Propene	3.1	-32.3	-33.0	4.4	-30.4	-31.2
1-butene	2.9	-32.1	-33.3	3.9	-31.0	-31.7
c-2-butene				3.9	-32.5	-33.3
t-2-butene				3.7	-31.2	-32.0
iso-butene	2.4	-31.9	-33.2	4.9	-29.9	-30.7
2-methyl-1-butene	2.1	-32.8	-33.4			

Table 11: Barriers and reaction enthalpies for vinyl + alkenes (current work). E_0 is difference between the zero-point corrected electronic energies of the transition state and reactants, ΔH_0 is the difference between the zero-point corrected electronic energies of the reactants and products, and ΔH_{298} is the reaction enthalpy at 298 K, all units in kcal/mol.

	methyl addition to unsubstituted center[a]		methyl addition to substituted center[a]		methyl addition to unsubstituted center[b]		methyl addition to substituted center[b]	
	E_0	ΔH_0	E_0	ΔH_0	E_a	ΔH_0	E_a	ΔH_0
Ethene	9.2	-21.0			7.3	-23.2		
Propene	8.8	-21.1	10.1	-20.1	7.0	-23.4	8.5	-22.2
1-butene					7.0	-23.0	8.1	-22.1
iso-butene	8.2	-20.5	11.2	-19.0	6.6	22.9	9.6	-21.0

Table 12: Barriers and reaction enthalpies for methyl + alkenes (from literature). [a] QCISD/6-31G(d)//G3X-RAD calculated 0K barriers (E_0) and reaction enthalpies (ΔH_0) in kcal/mol from Henry[24], and [b]fitted activation energies (E_a) and calculated reaction enthalpies (ΔH_{298K}) from CBS-QB3 calculations from Sabbe[25], in kcal/mol.

	$\frac{m^\dagger}{m}\frac{\sigma}{\sigma^\dagger}$	$\sqrt{\frac{\Theta_A\Theta_B\Theta_C}{\Theta_A^\dagger\Theta_B^\dagger\Theta_C^\dagger}}$
Ethene	4	22.3
Propene	2	8.4
1-butene	2	3.5
Cis-2-butene, trans-2-butene	4	4.6, 5.5
iso-butene	2	4.4

Table 13: Reaction Path Degeneracy and Rotational Effects. m is the number of energetically equivalent chiral states, σ is the external rotational symmetry number, Θ_A is the largest rotational constant of the alkene, and the superscript $\dagger$ denotes the transition state.

		$A\left(\frac{T}{1000\ [\mathrm{K}]}\right)^n = \frac{k_B T}{h}\frac{Q_{TS}}{Q_{AB}}$		Experiment, n=1.7		TST, n=1.7	
	E_0	A	n	A	E_a	A	E_a

ethene	3.7	1.2×10^{-12}	1.2	8.5×10^{-13}	3.1	1.1×10^{-12}	3.3
Propene, major	3.1	1.3×10^{-12}	1.7	1.3×10^{-12}	2.9	1.4×10^{-12}	3.1
1-butene, major	2.9	6.9×10^{-13}	1.9	8.6×10^{-13}	2.8	7.9×10^{-13}	3.2
cis-2-butene	3.9	1.3×10^{-12}	1.8			1.4×10^{-12}	4.1
trans-2-butene	3.7	1.3×10^{-12}	1.9			1.4×10^{-12}	3.9
2-butene, 50/50				9.2×10^{-13}	3.5		
iso-butene, major	2.4	4.2×10^{-13}	1.6	7.8×10^{-13}	2.8	5.5×10^{-13}	2.6
propene, minor	4.3	5.3×10^{-13}	1.6			5.7×10^{-13}	4.3
1-butene, minor	3.9	3.9×10^{-13}	1.9			4.9×10^{-13}	4.3
iso-butene, minor	4.8	2.2×10^{-13}	1.8			2.7×10^{-13}	5.2
2-methyl-1-butene, major	2.1	4.0×10^{-13}	1.6			4.1×10^{-13}	2.1

Table 14: Modified Arrhenius Parameters for Experimental Data and Theoretical Addition Rates. E_0 is the G3 barrier height at 0K in units of kcal/mol, n is the fitted temperature dependence of the A-factor of the major addition channel, A has units of cm^3/molecule/s, E_a has units of kcal/mol. 2-butene 50/50 corresponds to a 50% by volume blend of cis-2-butene and trans-2-butene, corresponding to the experimental gases. Major refers to addition to the unsubstituted carbon. TST corresponds to the calculated rate constants using transition state theory.

		$A\left(\frac{T}{1000\ [\mathrm{K}]}\right)^n = \frac{k_B T}{h}\frac{Q_{TS}}{Q_{AB}}$		TST Rate, n=2.8		Normalized Rate, n=2.8	
	E_0	A	n	A	E_a	A	E_a
propene	6.0	9.0×10^{-13}	2.7	8.3×10^{-13}	5.8	2.8×10^{-13}	5.8
1-butene	4.1	1.1×10^{-12}	2.8	1.1×10^{-12}	4.1	5.6×10^{-13}	4.1
cis-2-butene	5.1	1.6×10^{-12}	2.8	1.5×10^{-12}	5.0	2.5×10^{-13}	5.0
trans-2-butene	5.6	2.1×10^{-12}	2.8	1.9×10^{-12}	5.5	3.2×10^{-13}	5.5
iso-butene	5.4	1.6×10^{-12}	2.7	1.5×10^{-12}	5.2	2.5×10^{-13}	5.2

Table 15: Modified Arrhenius Parameters for H-Abstraction Rates. E_0 is the G3 barrier height at 0K in units of kcal/mol. The first A and n are the result from the fitting procedure in Equation (10) for the abstraction rate. The columns under TST Rate are the Arrhenius parameters for the calculated abstraction rate. A has units of cm^3/molecule/s, E_a has units of kcal/mol. The Normalized rates are the TST rates divided by the number of H-atoms which, upon abstraction, yield identical products.

References

(1) Tsang, W.; Hampson, R. F. *Journal of Physical and Chemical Reference Data* **1986**, *15*, 1087.

(2) Knyazev, V. D.; Slagle, I. R. *Journal of Physical Chemistry* **1996**, *100*, 16899.

(3) Richter, H.; Howard, J. B. *Progress in Energy and Combustion Science* **2000**, *26*, 565.

(4) Mebel, A. M.; Diau, E. W. G.; Lin, M. C.; Morokuma, K. *Journal of the American Chemical Society* **1996**, *118*, 9759.

(5) Fahr, A.; Stein, S. E. *Proc. Comb. Inst.* **1989**, *22*, 1023.

(6) Shestov, A. A.; Popov, K. V.; Slagle, I. R.; Knyazev, V. D. *Chemical Physics Letters* **2005**, *408*, 339.

(7) Ismail, H.; Goldsmith, C. F.; Abel, P. R.; Howe, P.-T.; Fahr, A.; Halpern, J. B.; Jusinski, L. E.; Georgievskii, Y.; Taatjes, C. A.; Green, W. H. *Journal of Physical Chemistry A* **2007**, *111*, 6843.

(8) Goldsmith, C. F.; Ismail, H.; Abel, P. R.; Green, W. H. *Proc. Comb. Inst.* **2009**, *32*, 139.

(9) Hunziker, H. E.; Kneppe, H.; McLean, A. D.; Siegbahn, P.; Wendt, H. R. *Canadian Journal of Chemistry* **1983**, *61*, 993.

(10) Pibel, C. D.; McIlroy, A.; Taatjes, C. A.; Alfred, S.; Patrick, K.; Halpern, J. B. *Journal of Chemical Physics* **1999**, *110*, 1841.

(11) Shahu, M.; Yang, C.-H.; Pibel, C. D.; McIlroy, A.; Taatjes, C. A.; Halpern, J. B. *Journal of Chemical Physics* **2002**, *116*, 8343.

(12) Ismail, H.; Abel, P. R.; Green, W. H.; Fahr, A.; Jusinski, L. E.; Knepp, A. M.; Zador, J.; Meloni, G.; Selby, T. M.; Osborn, D. L.; Taatjes, C. A. *Journal Of Physical Chemistry A* **2009**, *113*, 1278.

(13) Curtiss, L. A.; Raghavachari, K.; Redfern, P. C.; Rassolov, V.; Pople, J. A. *Journal of Chemical Physics* **1998**, *109*, 7764.

(14) Pitzer, K. S.; Gwinn, W. D. *Journal of Chemical Physics* **1942**, *10*, 428.

(15) Johnston, H. S.; Heicklen, J. *Journal of Physical Chemistry* **1962**, *66*, 532.

(16) Miller, J. A.; Klippenstein, S. J.; Raffy, C. *Journal of Physical Chemistry A* **2002**, *106*, 4904.

(17) Miller, J. A.; Klippenstein, S. J. *Journal of Physical Chemistry A* **2003**, *107*, 2680.

(18) Barker, J. R.; Ortiz, N. F.; Preses, J. M.; Lohr, L. L.; Maranzana, A.; Stimac, P. J. MultiWell-2.08 Software University of Michigan, Ann Arbor, MI, 2007.

(19) Frisch, M. J.; Trucks, G. W.; Schlegel, H. B.; Scuseria, G. E.; Robb, M. A.; Cheeseman, J. R.; Montgomery, J., J. A.; Vreven, T.; Kudin, K. N.; Burant, J. C.; Millam, J. M.; Iyengar, S. S.; Tomasi, J.; Barone, V.; Mennucci, B.; Cossi, M. S., G.; Rega, N.; Petersson, G. A.; Nakatsuji, H.; Hada, M.; Ehara, M.; Toyota, K.; Fukuda, R.; Hasegawa, J.; Ishida, M.; Nakajima, T.; Honda, Y.; Kitao, O.; Nakai, H.; Klene, M.; Li, X.; Knox, J. E.; Hratchian, H. P.; Cross, J. B.; Bakken, V.; Adamo, C.; Jaramillo, J.; Gomperts, R.; Stratmann, R. E.; Yazyev, O.; Austin, A. J.; Cammi, R.; Pomelli, C.;

Ochterski, J. W.; Ayala, P. Y.; Morokuma, K.; Voth, G. A.; Salvador, P.; Dannenberg, J. J.; Zakrzewski, V. G.; Dapprich, S.; Daniels, A. D.; Strain, M. C.; Farkas, O.; Malick, D. K.; Rabuck, A. D.; Raghavachari, K.; Foresman, J. B.; Ortiz, J. V.; Cui, Q.; Baboul, A. G.; Clifford, S.; Cioslowski, J.; Stefanov, B. B.; Liu, G.; Liashenko, A.; Piskorz, P.; Komaromi, I.; Martin, R. L.; Fox, D. J.; Keith, T.; Al-Laham, M. A.; Peng, C. Y.; Nanayakkara, A.; Challacombe, M.; Gill, P. M. W.; Johnson, B.; Chen, W.; Wong, M. W.; Gonzalez, C.; Pople, J. A. In *Gaussian 03*; Gaussian, Inc., 2004.

(20) Werner, H.-J.; Knowles, P. J.; Lindh, R.; Manby, F. R.; Schuetz, M.; others, a. MOLPRO, version 2006.1, a package of ab initio programs; see http://www.molpro.net, 2006.

(21) Klippenstein, S. J.; Wagner, A. F.; Dunbar, R. C.; Wardlaw, D. M.; Robertson, S. H.; Miller, J. A. *VARIFLEX* **2002**.

(22) Miller, J. A.; Klippenstein, S. J. *Journal Of Physical Chemistry A* **2001**, *105*, 7254.

(23) Fischer, H.; Radom, L. *Angewandte Chemie-International Edition* **2001**, *40*, 1340.

(24) Henry, D. J.; Coote, M. L.; Gomez-Balderas, R.; Radom, L. *Journal of the American Chemical Society* **2004**, *126*, 1732.

(25) Sabbe, M. K.; Reyniers, M. F.; Van Speybroeck, V.; Waroquier, M.; Marin, G. B. *Chemphyschem* **2008**, *9*, 124.

(26) Sabbe, M., K, Personal communication with author.

(27) Lias, S. G.; Bartmess, J. E.; Liebman, J. F.; Holmes, J. L.; Levin, R. D.; Mallard, W. G. "Ion Energetics Data". In *NIST Chemistry WebBook, NIST Standard Reference Database, http://webbook.nist.gov;* Mallard, P. J. L. a. W. G., Ed.; National Institute of Standards and Technology: Gaithersburg, 2009; Vol. 69.

(28) DeSain, J. D.; Jusinski, L. E.; Taatjes, C. A. *Physical Chemistry Chemical Physics* **2006**, *8*, 2240.